

A study of 315 glitches in the rotation of 102 pulsars

C.M. Espinoza^{1*}, A.G. Lyne¹, B.W. Stappers¹ and M. Kramer^{1,2}

¹*Jodrell Bank Centre for Astrophysics, School of Physics and Astronomy, The University of Manchester, Manchester M13 9PL, UK*

²*Max-Planck-Institut für Radioastronomie, Auf dem Hgel 69, 53121 Bonn, Germany*

ABSTRACT

The rotation of more than 700 pulsars has been monitored using the 76-m Lovell Telescope at Jodrell Bank. Here we report on a new search for glitches in the observations, revealing 128 new glitches in the rotation of 63 pulsars. Combining these new data with those already published we present a database containing 315 glitches in 102 pulsars. The database was used to study the glitch activity among the pulsar population, finding that it peaks for pulsars with a characteristic age $\tau_c \sim 10$ kyr and decreases for longer values of τ_c , disappearing for objects with $\tau_c > 20$ Myr. The glitch activity is also smaller in the very young pulsars ($\tau_c \lesssim 1$ kyr). The cumulative effect of glitches, a collection of instantaneous spin up events, acts to reduce the regular long term spindown rate $|\dot{\nu}|$ of the star. The percentage of $|\dot{\nu}|$ reversed by glitch activity was found to vary between 0.5% and 1.6% for pulsars with spindown rates $|\dot{\nu}|$ between 10^{-14} and $3.2 \times 10^{-11} \text{ Hz s}^{-1}$, decreasing to less than 0.01% at both higher and lower spindown rates. These ratios are interpreted in terms of the amount of superfluid involved in the generation of glitches. In this context the activity of the youngest pulsar studied, the Crab pulsar may be explained by quake-like activity within the crust. Pulsars with low spindown rates seem to exhibit mostly small glitches, matching well the decrease of their crustal superfluid.

Through the analysis of glitch sizes it was found that the particular glitching behaviour of PSR J0537–6910 and the Vela pulsar may be shared by most Vela-like pulsars. These objects present most of their glitches with characteristic frequency and frequency derivative jumps, occurring at regular intervals of time. Their behaviour is different from other glitching pulsars of similar characteristic age.

Key words: stars: neutron – pulsars: general

1 INTRODUCTION

Pulsar timing, the method by which the rotation of pulsars is described, is a high precision discipline. Often, with a very simple model it is possible to predict every turn of the star over many years, with an accuracy of a few microseconds, or better. This accuracy makes it possible to detect and measure very small perturbations affecting the normal rotation of the star, supplying information about processes inside and outside the pulsar. Two types of timing irregularity have been recognised which still remain to be well understood: timing noise and glitches. Timing noise refers to unexpected, thus unmodelled, features in the timing residuals relative to a simple slowdown model. It can be described as a random wandering of the residuals, sometimes presenting a clear quasiperiodic behaviour (Hobbs et al. 2010). Perhaps most, if not all, of this has recently been shown to arise in instabilities in the pulsar magnetosphere which result in steps

in the slowdown rate (Lyne et al. 2010). On the other hand, glitches are discrete changes on the pulsar rotation rate, often followed by a relaxation. Our knowledge of the physics behind glitches has increased fairly slowly (Glampedakis & Andersson 2009), probably due to the lack of relevant observational input to constrain the physical models. The study of glitches is important, as they are one of the very few instances through which we can study the interior of a neutron star and the properties of matter at super nuclear density (Baym et al. 1969). They also have proved to play an important role in the long-term spin evolution of young pulsars (Lyne et al. 1996), and, if the gravitational radiation related to glitches was to be detected, relevant information on the interior and orientation of the pulsar could be obtained (van Eysden & Melatos 2008).

Glitches are rare events of very short duration, seen in the data as sudden jumps in rotational frequency (ν), normally ranging between $10^{-3} \mu\text{Hz}$ and $\sim 100 \mu\text{Hz}$. Following a glitch, the pulsar sometimes enters a stage of recovery, in which the rotation frequency decays towards the pre-glitch

* E-mail: cme@jb.man.ac.uk

value. These recoveries have been interpreted as a signature of the presence of a superfluid in the interior of the star (Baym et al. 1969). Glitches are thought to be the result of a rapid transfer of angular momentum between this inner superfluid and the outer crust, to which the neutron star magnetosphere is attached and whose radiation we observe. The crust is thought to be slowed down by electromagnetic torques provided by the magnetosphere, and because the frictional forces between these two layers are small, the superfluid keeps rotating faster than the crust, with an angular velocity lag which is reduced during a glitch (e.g. Anderson & Itoh 1975; Alpar et al. 1984) and which subsequently recovers. No change of pulse profile or radio flux density has ever been reported to be associated with a glitch in a normal radio pulsar. The coincidence observed between glitches and enhancement in X-rays flux in a few magnetars (Woods et al. 2004; Israel et al. 2007; Dib et al. 2007), and particularly in the high magnetic field X-ray pulsar PSR J1846–0258 (Kuiper & Hermsen 2009; Livingstone et al. 2010), seems to belong purely to very high magnetic field neutron stars. Outburst episodes, thought to be caused by magnetic field decay (Thompson & Duncan 1995; Thompson & Duncan 1996), are often detected from these objects, but are not always found associated with glitches, as glitches are not always related to X-ray flux variations (Dib et al. 2008).

As a result of regular monitoring of a large number of pulsars, a few of which glitch relatively often, some trends in glitching behaviour have been revealed. If a glitch occurs when the angular velocity difference between the two main inner components is reduced, then the glitch activity should decay with the spindown rate of the pulsar, $|\dot{\nu}|$ (McKenna & Lyne 1990). This has been proven by Lyne et al. (2000), who showed that the rate of spin-up due to glitches is proportional to $|\dot{\nu}|$, for pulsars with $|\dot{\nu}|$ between $\sim 10^{-14} \text{ Hz s}^{-1}$ and $\sim 10^{-11} \text{ Hz s}^{-1}$. The characteristic age $\tau_c = -\nu/2\dot{\nu}$ has also been used as a parameter to describe the glitch activity of pulsars, indicating that activity peaks for $\tau_c \sim 10^4 \text{ yr}$ and decreases for older pulsars (McKenna & Lyne 1990; Wang et al. 2000). Additionally, it has been observed that very young pulsars ($\tau_c < 2 \times 10^3 \text{ yr}$) also have little glitch activity (Shemar & Lyne 1996), an effect attributable to their likely higher internal temperature (McKenna & Lyne 1990).

In this paper we present the results of a new search for glitches performed using the Jodrell Bank pulsar timing database. Together with 186 glitches that can be found in the literature, the 128 new glitches found in this work are used to study the glitching behaviour of pulsars. Section 2 describes the data and section 3 explains how these were analysed to extract the glitches and their main parameters. In section 4 the large glitch database is presented, and then analysed in the next section. Finally, sections 6 and 7 present the discussion and a summary of the conclusions, respectively.

2 THE JODRELL BANK PULSAR TIMING DATABASE

The Jodrell Bank timing database comprises observations of more than 700 hundred pulsars, carried out at Jodrell Bank observatory (JBO) since 1978, and it is described by Hobbs et al. (2004). In summary, observations have mostly

been performed with the 76-m Lovell telescope, with some complementary observations made using the 30-m MkII and 42-ft telescopes. Every pulsar is observed at typical intervals of 2 to 10 days in a 64-MHz band centred on 1404 MHz, using an analogue filter-bank. Occasionally, observations were also carried out in a band centred at 610 MHz.

3 CHARACTERISING GLITCHES

Pulsar timing, the method by which the rotation of pulsars is described, is based on the analysis of the times of arrival (TOAs) of the pulses from the pulsar at the observatory. These TOAs are obtained by matching the observed pulse profile with a standard, representative template. TOAs are corrected for the motion of the observatory around the Solar System barycentre and then compared with a simple slow-down model describing the rotation of the star, that predicts that the pulse number N , arriving at time t is given by

$$N = \nu_0(t - t_0) + \frac{1}{2}\dot{\nu}_0(t - t_0)^2 + \frac{1}{6}\ddot{\nu}_0(t - t_0)^3 + \dots, \quad (1)$$

where ν_0 , $\dot{\nu}_0$ and $\ddot{\nu}_0$ are the rotational frequency and its first two derivatives at the epoch t_0 . The model will give integer numbers if the rotational parameters are exactly correct. The fractional part of N multiplied by the period of the pulsar is called a timing residual. The frequency and its derivatives at t_0 are determined by minimising the timing residuals, which in an ideal case are expected to be normally distributed around zero.

The signature of a glitch in a plot of timing residuals with epoch is normally characterised by the sudden onset of a continuous increase towards negative values, relative to an ephemeris based upon preceding data, as can be seen in the first panel of Fig. 1, where a relatively small glitch is shown. A fit of ν , $\dot{\nu}$ and $\ddot{\nu}$ to pre-glitch data describes the rotation of the pulsar well, but after the glitch a new set of parameters is needed in order to minimise the residuals satisfactorily. Panel (b) of the figure shows the residuals obtained if we attempt to fit the whole data-set in the plot with only one set of parameters. The glitch is visible with a characteristic shape, showing a sharp cusp-like feature which suggests that a single-epoch event happened at that time. Such a pattern is characteristic of glitches, while timing noise is normally seen as rounded wave-like features in the residuals, without a preferred direction and without single-epoch events.

3.1 Glitch sizes and recoveries

Glitches can also be seen in a frequency residuals plot, obtained after removing the main slope of the frequency. Fig. 1(c) shows the evolution of the frequency residuals through a glitch. The glitch is observed to be a sudden positive step in frequency, in this case followed by a negative change of the slope. The size of the frequency step is probably the main way to characterise a glitch. It is normally expressed as the fractional quantity $\Delta\nu/\nu$, where $\Delta\nu$ is the difference between the frequency after and before the glitch. Detected glitch sizes range between 10^{-11} and 10^{-5} . Glitches in the Crab pulsar are all smaller than 200×10^{-9} while in the Vela pulsar almost all glitches are larger than 1000×10^{-9} (Wong et al. 2001; McCulloch et al. 1990).

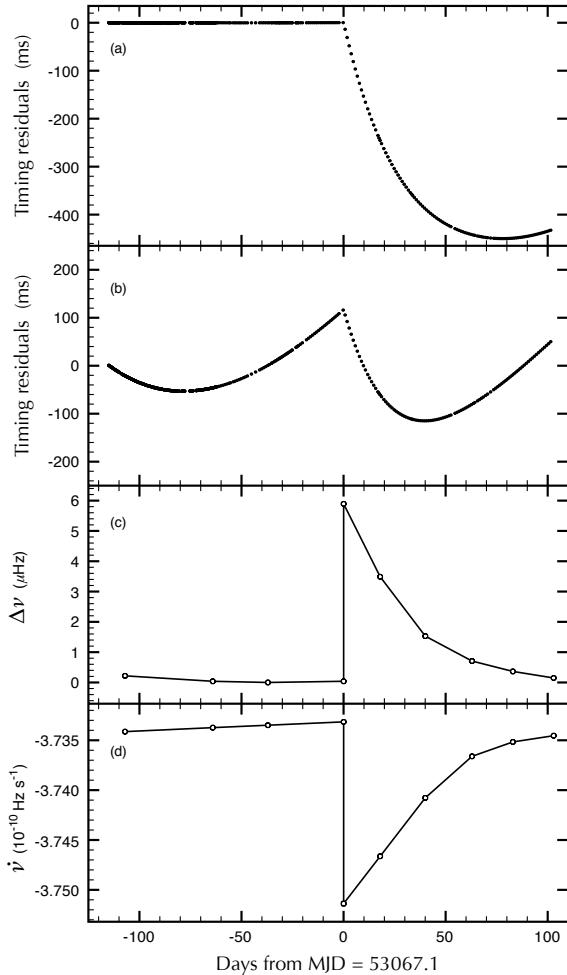


Figure 1. A glitch in the data of PSR B0531+21, the Crab pulsar. It occurred around MJD 53067 and had a fractional frequency jump of $\Delta\nu/\nu = 5.33 \pm 0.05 \times 10^{-9}$; a small glitch. (a) The timing residuals relative to a slowdown model with two frequency derivatives when fitting data only up to the glitch date. (b) Timing residuals after fitting all data in the plot; note that the glitch feature is still visible. Both these panels have the same scale, covering 500 ms. (c) Frequency residuals, obtained by subtracting the main slope given by an average $\dot{\nu}$. (d) The behaviour of $\dot{\nu}$ through the glitch.

Most glitches are followed by an increase in the spin-down rate $|\dot{\nu}|$, which may subsequently recover towards pre-glitch values. Panel (d) of Fig. 1 shows the evolution of $\dot{\nu}$ through a glitch. Large glitches and their recoveries are easily visualised in a $\dot{\nu}$ -plot. Recoveries can sometimes be modelled using an exponential function with a typical time constant of ~ 100 days, plus a longer time-scale term, which can either be represented by a second exponential with a larger time constant ($\sim 1,000$ days) or by a simple linear decay of $|\dot{\nu}|$ (Shemar & Lyne 1996). The step in frequency derivative at a glitch is expressed as the fractional quantity $\Delta\dot{\nu}/\dot{\nu}$ and detected values range between 10^{-4} and ~ 1 . Our ability to measure $\Delta\dot{\nu}$ depends strongly on how well sampled the pulsar rotation is around the glitch. Particularly, if a set of exponentials are being fitted, the reliability of $\Delta\dot{\nu}$ will depend on the interval size of the post-glitch data used

to fit, and of course on the capacity of the model to describe the data (see Zou et al. (2008), concerning PSR B1737–30, and Wong et al. (2001), concerning the Crab pulsar). The results presented in this paper do not involve fitting of short-term recoveries because their parameters depend so critically upon the usually poorly known glitch epoch.

Frequency and $\dot{\nu}$ plots are produced by performing fits of ν , $\dot{\nu}$ and sometimes $\ddot{\nu}$ to consecutive overlapping groups of TOAs, each group typically covering a 200 days interval. To produce a series of ν and $\dot{\nu}$ values the time interval is generally shifted by 100 days and the fit performed again.

3.2 Glitch detection

In our searches, all glitches were detected by visual inspection of the phase residuals, relative to a slowdown model with a maximum of two frequency derivatives. Any feature looking similar to those in the top two panels of Fig. 1 was considered as a possible glitch, and explored in detail. Medium size and large glitches ($\Delta\nu/\nu \geq 50 \times 10^{-9}$) always have a clear signature in the timing residuals; they are obvious and easy to differentiate from timing noise.

Small glitches are more difficult to identify. The smallest glitch ever detected is the one in the millisecond pulsar PSR B1821–24, with a fractional frequency change of only $0.0095(1) \times 10^{-9}$ (Cognard & Backer 2004). In spite of its small size, this glitch was easy to detect, due to the natural rotational stability and small errors in the TOAs of a millisecond pulsar. In contrast, for pulsars with higher levels of timing noise and/or larger errors in the TOAs the amplitude of the glitch signature could be smaller than the noise variations, making detection more uncertain. The size of the smallest detectable glitch depends strongly on the timing noise levels of the particular pulsar, the signal-to-noise ratio of the TOAs, and also on how often the observations were made. If the TOAs are typically separated by a time longer than the glitch recovery time-scales, or there is a gap with no data, then the detection of a small glitch may not be possible, or if it is, it might be difficult to get good estimates of its epoch and size.

3.3 Determination of Glitch parameters

To estimate the glitch epoch and the size of jumps in $\Delta\nu$ and $\Delta\dot{\nu}$, ephemerides describing the data immediately before and after the glitch were built, by fitting ν , $\dot{\nu}$ and $\ddot{\nu}$, and setting the epoch of both ephemerides near to an approximate glitch epoch. The two solutions are then compared, and the epoch at which the phases are the same is taken as the glitch epoch. For a large glitch (e.g. $\Delta\nu/\nu > 1000 \times 10^{-9}$) there could be several epochs for which this is true between the TOA's T_1 and T_2 that surround the glitch. In this case the glitch epoch was taken to be the average of T_1 and T_2 , and the error was estimated as $(T_2 - T_1)/4$, which corresponds to 1- σ of a square distribution between T_1 and T_2 . The steps $\Delta\nu$ and $\Delta\dot{\nu}$ are found by taking the difference of the values from the two solutions at the estimated glitch epoch. The post-glitch ephemeris was always built intending to describe the pulsar rotation immediately after the glitch, ideally covering only 30 or 50 days. Unfortunately this was not always possible, because the sampling on some pulsars is rather poor, and longer intervals had to be used in those cases.

Table 1. All glitches, previously published and found in this work. For re-analysed glitches the new values are shown, and the original references are given in the last column. Errors are given in parentheses on units of the last quoted digit. Visit <http://www.jb.man.ac.uk/pulsar/glitches.html> for an online and up-to-date version of this Table.

Name	J-name	No. Glt's	MJD days	$\Delta\nu/\nu$ 10^{-9}	$\Delta\dot{\nu}/\dot{\nu}$ 10^{-3}	References
4U 0142+61	0146+6145	1	51141(248)	650(150)	14(5)	Morii et al. (2005)
B0154+61	0157+6212	1	48512(5)	4(1)	-11(6)	t, also in Krawczyk et al. (2003)
J0205+6449	0205+6449	1	52555(8)	340(110)	5(1)	Livingstone et al. (2009)
J0205+6449	0205+6449	2	52920(72)	3800(400)	12(1)	Livingstone et al. (2009)
B0355+54	0358+5413	1	46082(4)	6(1)	6(5)	t, also in Lyne (1987)
B0355+54	0358+5413	2	46470(18)	4366(1)	430(154)	t, also in Lyne (1987)
B0355+54	0358+5413	3	51679(15)	0.06(4)	0.0(2)	t, also in Janssen & Stappers (2006)
B0355+54	0358+5413	4	51969(1)	0.7(2)	15(7)	t, also in Janssen & Stappers (2006)
B0355+54	0358+5413	5	52943(3)	2(1)	-39(76)	t, also in Janssen & Stappers (2006)
B0355+54	0358+5413	6	53209(2)	1(1)	207(70)	t, also in Janssen & Stappers (2006)
B0458+46	0502+4654	1	52616(2)	0.33(2)	0.7(2)	t
B0525+21	0528+2200	1	42051.5(3)	1.9(2)	13(5)	t, also in Downs (1982)
B0525+21	0528+2200	2	52296(1)	2.3(2)	7(2)	Janssen & Stappers (2006)
B0525+21	0528+2200	3	53379	0.2(1)	--	Janssen & Stappers (2006)
B0531+21	0534+2200	1	40491.84(3)	7.2(4)	0.44(4)	t, also in Lohsen (1981)
B0531+21	0534+2200	2	41161.98(4)	1.9(1)	0.17(1)	t, also in Lohsen (1981)
B0531+21	0534+2200	3	41250.32(1)	2.1(1)	0.11(1)	t, also in Lohsen (1981)
B0531+21	0534+2200	4	42447.26(4)	35.7(3)	1.6(1)	t, also in Lohsen (1981)
B0531+21	0534+2200	5	46663.69(3)	6(1)	0.5(1)	t, also in Lyne & Pritchard (1987)
B0531+21	0534+2200	6	47767.504(3)	81.0(4)	3.4(1)	t, also in Lyne et al. (1992)
B0531+21	0534+2200	7	48945.6(1)	4.2(2)	0.32(3)	t, also in Lyne et al. (1993), Wong et al. (2001)
B0531+21	0534+2200	8	50020.04(2)	2.1(1)	0.20(1)	t, also in Wong et al. (2001)
B0531+21	0534+2200	9	50260.031(4)	31.9(1)	1.73(3)	t, also in Wong et al. (2001)
B0531+21	0534+2200	10	50458.94(3)	6.1(4)	1.1(1)	t, also in Wong et al. (2001)
B0531+21	0534+2200	11	50489.7(2)	0.8(3)	-0.2(1)	t, also in Wong et al. (2001)
B0531+21	0534+2200	12	50812.59(1)	6.2(2)	0.62(4)	t, also in Wong et al. (2001)
B0531+21	0534+2200	13	51452.02(1)	6.8(2)	0.7(1)	t, also in Wong et al. (2001)
B0531+21	0534+2200	14	51740.656(2)	25.1(3)	2.9(1)	t
B0531+21	0534+2200	15	51804.75(2)	3.5(1)	0.53(3)	t
B0531+21	0534+2200	16	52084.072(1)	22.6(1)	2.07(3)	t
B0531+21	0534+2200	17	52146.7580(3)	8.87(5)	0.57(1)	t
B0531+21	0534+2200	18	52498.257(2)	3.4(1)	0.70(2)	t
B0531+21	0534+2200	19	52587.20(1)	1.7(1)	0.5(1)	t
B0531+21	0534+2200	20	53067.0780(2)	214(1)	6.2(2)	t
B0531+21	0534+2200	21	53254.109(2)	4.9(1)	0.16(5)	t
B0531+21	0534+2200	22	53331.17(1)	2.8(2)	0.7(1)	t
B0531+21	0534+2200	23	53970.1900(3)	21.8(2)	3.1(1)	t
B0531+21	0534+2200	24	54580.38(1)	4.7(1)	0.2(1)	t
J0537-6910	0537-6910	1	51286(9)	681(65)	0(1)	Middleditch et al. (2006)
J0537-6910	0537-6910	2	51569(7)	449(8)	0.8(5)	Middleditch et al. (2006)
J0537-6910	0537-6910	3	51711(7)	315(9)	1(1)	Middleditch et al. (2006)
J0537-6910	0537-6910	4	51826(7)	140(7)	0(1)	Middleditch et al. (2006)
J0537-6910	0537-6910	5	51881(6)	141(20)	0.2(3)	Middleditch et al. (2006)
J0537-6910	0537-6910	6	51960(5)	456(46)	1(1)	Middleditch et al. (2006)
J0537-6910	0537-6910	7	52171(8)	185(6)	0.64(3)	Middleditch et al. (2006)
J0537-6910	0537-6910	8	52242(8)	427(6)	0.17(4)	Middleditch et al. (2006)
J0537-6910	0537-6910	9	52386(6)	168(20)	0.6(2)	Middleditch et al. (2006)
J0537-6910	0537-6910	10	52453(7)	217(30)	0.3(4)	Middleditch et al. (2006)
J0537-6910	0537-6910	11	52545(6)	421(18)	0.4(2)	Middleditch et al. (2006)
J0537-6910	0537-6910	12	52740(5)	144(6)	0.56(3)	Middleditch et al. (2006)
J0537-6910	0537-6910	13	52819(4)	256(16)	0.4(2)	Middleditch et al. (2006)
J0537-6910	0537-6910	14	52887(5)	234(23)	0.6(3)	Middleditch et al. (2006)
J0537-6910	0537-6910	15	53014(10)	338(10)	0.7(1)	Middleditch et al. (2006)
J0537-6910	0537-6910	16	53125(3)	18(14)	0.6(2)	Middleditch et al. (2006)
J0537-6910	0537-6910	17	53145(3)	392(8)	-0.1(2)	Middleditch et al. (2006)
J0537-6910	0537-6910	18	53288(2)	395(10)	0.7(1)	Middleditch et al. (2006)
J0537-6910	0537-6910	19	53446(2)	259(16)	0.7(1)	Middleditch et al. (2006)
J0537-6910	0537-6910	20	53551(4)	322(26)	0.6(2)	Middleditch et al. (2006)
J0537-6910	0537-6910	21	53699(4)	402(8)	0.6(2)	Middleditch et al. (2006)
J0537-6910	0537-6910	22	53860(2)	236(20)	0.6(2)	Middleditch et al. (2006)
J0537-6910	0537-6910	23	53951(2)	18(20)	--	Middleditch et al. (2006)
B0540-69	0540-6919	1	51335(12)	1.4(2)	0.133(2)	Livingstone et al. (2005)
B0559-05	0601-0527	1	51665.2(1)	0.19(5)	-0.7(1)	t
J0631+1036	0631+1036	1	50183.5(2)	4.7(1)	-0.7(1)	t
J0631+1036	0631+1036	2	50480.1(1)	4.2(2)	0.1(2)	t
J0631+1036	0631+1036	3	50608.277(1)	57.3(1)	1.15(5)	t
J0631+1036	0631+1036	4	50729(1)	1662.7(1)	3.5(2)	t
J0631+1036	0631+1036	5	51909.69(5)	1.4(1)	0.26(4)	t
J0631+1036	0631+1036	6	52852.50(1)	17.6(1)	2.48(4)	t

... continued on next page

Table 1 – continued

Name	J-name	No. Glt's	MJD days	$\Delta\nu/\nu$ 10^{-9}	$\Delta\dot{\nu}/\dot{\nu}$ 10^{-3}	References
J0631+1036	0631+1036	7	53230.1(1)	1.6(1)	0.4(1)	t
J0631+1036	0631+1036	8	53366(1)	1.9(1)	0.28(5)	t
J0631+1036	0631+1036	9	53622.6(2)	1.1(5)	0.2	t
J0631+1036	0631+1036	10	54099(2)	0.4(1)	-0.2(1)	t
J0631+1036	0631+1036	11	54170.4(1)	1.6(1)	-0.1(1)	t
J0631+1036	0631+1036	12	54632.530(2)	43.2(1)	3.3(2)	t
J0633+1746	0633+1746	1	50382	0.6	—	Jackson et al. (2002)
B0656+14	0659+1414	1	50197(8)	0.6(4)	0.3(5)	t
B0656+14	0659+1414	2	51017(3)	1.3(1)	1.8(6)	t
B0727-18	0729-1836	1	51421.9(5)	1.0(5)	-2(3)	t
B0727-18	0729-1836	2	52150(3)	4(1)	6(2)	t
J0729-1448	0729-1448	1	52010(1)	24.8(4)	1.6(3)	t
J0729-1448	0729-1448	2	54317.7(2)	23(1)	4(3)	t
J0729-1448	0729-1448	3	54483.6(3)	13(1)	1(1)	t
J0729-1448	0729-1448	4	54592(1)	12(1)	-2(2)	t
J0729-1448	0729-1448	5	54687(3)	6676(9)	54(5)	t
B0740-28	0742-2822	1	47625(3)	1.2(1)	-0.8(3)	t, also in D'Alessandro et al. (1993)
B0740-28	0742-2822	2	48331.7(3)	1.2(1)	-1.3(5)	t, also in D'Alessandro et al. (1993)
B0740-28	0742-2822	3	51770(20)	1.0(3)	0.9(2)	Janssen & Stappers (2006)
B0740-28	0742-2822	4	52028(2)	3.7(2)	4(1)	t, also in Janssen & Stappers (2006)
B0740-28	0742-2822	5	53083.1(5)	1.7(2)	-1(1)	t, also in Janssen & Stappers (2006)
B0740-28	0742-2822	6	53467.7(3)	1.8(1)	4.6(5)	t, also in Janssen & Stappers (2006)
B0740-28	0742-2822	7	55020.469(4)	92(2)	-372(96)	t
B0756-15	0758-1528	1	49963(4)	0.11(3)	2(2)	t
B0833-45	0835-4510	1	40280(4)	2340(10)	10(1)	Downs (1981)
B0833-45	0835-4510	2	41192(8)	2050(30)	15(6)	Downs (1981)
B0833-45	0835-4510	3	41312(4)	12(2)	3(6)	Cordes et al. (1988)
B0833-45	0835-4510	4	42683(3)	1990(10)	11(7)	Downs (1981)
B0833-45	0835-4510	5	43693(12)	3060(60)	18(9)	Downs (1981)
B0833-45	0835-4510	6	44888.4(4)	1145(3)	49(4)	Cordes et al. (1988)
B0833-45	0835-4510	7	45192(1)	2050(10)	23(1)	Cordes et al. (1988)
B0833-45	0835-4510	8	46257.228(1)	1601(1)	17(1)	McCulloch et al. (1987)
B0833-45	0835-4510	9	47519.8036(1)	1805(1)	77(6)	McCulloch et al. (1990)
B0833-45	0835-4510	10	48457.382(1)	2715(2)	600(60)	Flanagan (1991)
B0833-45	0835-4510	11	49559.0(2)	835(2)	0(5)	Flanagan & McCulloch (1994)
B0833-45	0835-4510	12	49591.2	199(2)	120(20)	Flanagan (1994)
B0833-45	0835-4510	13	50369.345(2)	2110(17)	5.95(3)	Wang et al. (2000)
B0833-45	0835-4510	14	51559.319(1)	3085.72(4)	6.736(1)	Dodson et al. (2002)
B0833-45	0835-4510	15	53193	2100	—	Dodson et al. (2004)
B0833-45	0835-4510	16	53960	2620	230(40)	Flanagan & Buchner (2006)
B1046-58	1048-5832	1	48944(2)	19(2)	0.3(1)	Wang et al. (2000)
B1046-58	1048-5832	2	49034(9)	3000(10)	3.7(1)	Wang et al. (2000)
B1046-58	1048-5832	3	50791.49(5)	768(1)	14(5)	Urama (2002)
1E 1048 ^a	1048-5937	1	52386(2)	2900(100)	76(4)	Dib et al. (2009)
1E 1048	1048-5937	2	54185.9(1)	16300(200)	-111(74)	Dib et al. (2009)
J1105-6107	1105-6107	1	50417(16)	279.7(2)	4.63(4)	Wang et al. (2000)
J1105-6107	1105-6107	2	50610(3)	2(3)	0.19(1)	Wang et al. (2000)
J1119-6127	1119-6127	1	51398(4)	4.4(4)	0.04(1)	Camilo et al. (2000)
J1123-6259	1123-6259	1	49705.87(1)	749(1)	1.0(4)	Wang et al. (2000)
J1141-3322	1141-3322	1	50521.31(3)	0.4(1)	-4(5)	t
B1259-63	1302-6350	1	50691(1)	3.2(1)	2.5(1)	Wang et al. (2004)
B1325-43	1328-4357	1	43590(24)	116	—	Newton et al. (1981)
B1338-62	1341-6220	1	47989(21)	1509(1)	0.2(1)	Wang et al. (2000)
B1338-62	1341-6220	2	48453(12)	23(7)	-0.5(1)	Wang et al. (2000)
B1338-62	1341-6220	3	48645(10)	996(3)	0.7(1)	Wang et al. (2000)
B1338-62	1341-6220	4	49134(22)	13.2(13)	0.6(2)	Wang et al. (2000)
B1338-62	1341-6220	5	49363(130)	146(38)	0.7(2)	Wang et al. (2000)
B1338-62	1341-6220	6	49523(17)	37(35)	-0.6(1)	Wang et al. (2000)
B1338-62	1341-6220	7	49766(2)	15(2)	-0.3(1)	Wang et al. (2000)
B1338-62	1341-6220	8	49904(16)	31(1)	-1.9(4)	Wang et al. (2000)
B1338-62	1341-6220	9	50008(16)	1648(3)	3.3(4)	Wang et al. (2000)
B1338-62	1341-6220	10	50322(1)	30(1)	0.6(1)	Wang et al. (2000)
B1338-62	1341-6220	11	50529(1)	23(1)	1.0(4)	Wang et al. (2000)
B1338-62	1341-6220	12	50683(13)	708(1)	1.2(3)	Wang et al. (2000)
J1357-6429	1357-6429	1	52021(8)	2428(1)	6.3(1)	t, also in Camilo et al. (2004)
B1508+55	1509+5531	1	41732(58)	0.2(1)	-6(1)	Manchester & Taylor (1974)
B1530+27	1532+2745	1	49732(3)	0.29(4)	-1(2)	t
B1535-56	1539-5626	1	48165(15)	2793(1)	1(1)	Johnston et al. (1995)
B1610-50	1614-5048	1	49803(16)	6460(80)	9.7(2)	Wang et al. (2000)
J1617-5055	1617-5055	1	46960(760)	600(5)	—	Torii et al. (2000)
B1641-45	1644-4559	1	43390(63)	191(1)	2(1)	Manchester et al. (1978)
B1641-45	1644-4559	2	46453(35)	803.6(1)	0.5(3)	Flanagan (1993)

... continued on next page

Table 1 – *continued*

Name	J-name	No. Glt's	MJD days	$\Delta\nu/\nu$ 10^{-9}	$\Delta\dot{\nu}/\dot{\nu}$ 10^{-3}	References
B1641–45	1644–4559	3	47589(4)	1.61(4)	1.1(1)	Flanagan (1993)
CXO J1647 ^b	1647–4552	1	53999	65000(3000)	—	Israel et al. (2007)
B1702–19	1705–1906	1	48902.1(5)	0.4(1)	1(1)	t
J1705–3423	1705–3423	1	51956(1)	0.59(4)	0.7(5)	t
J1705–3423	1705–3423	2	54408(2)	0.57(4)	3(1)	t
B1706–44	1709–4429	1	48775(15)	2057(2)	4.0(1)	Johnston et al. (1995)
1RXS J1708 ^c	1708–4009	1	51445	561(33)	5(3)	Dib et al. (2008)
1RXS J1708	1708–4009	2	52016	4202(44)	620(1)	Dib et al. (2008)
1RXS J1708 ^{c1}	1708–4009	3	52990	308(44)	0.0	Dib et al. (2008)
1RXS J1708 ^{c2}	1708–4009	4	53366	572(66)	12(8)	Dib et al. (2008)
1RXS J1708	1708–4009	5	53549	2707(99)	12(12)	Dib et al. (2008)
1RXS J1708 ^{c3}	1708–4009	6	53636	737(33)	–36(3)	Dib et al. (2008)
B1717–16	1720–1633	1	51169(1)	1.5(2)	8(3)	t
B1718–35	1721–3532	1	49971(2)	7.5(3)	0.3(4)	t
B1727–33	1730–3350	1	48000(10)	3033(8)	4(6)	Johnston et al. (1995)
B1727–33	1730–3350	2	52107(19)	3202(1)	5.9(1)	t
B1727–47	1731–4744	1	49387.2(1)	137(1)	1.5(4)	t, also in D'Alessandro & McCulloch (1997)
B1727–47	1731–4744	2	50718.1(1)	4.4(2)	4.0(5)	t, also in Wang et al. (2000)
B1727–47	1731–4744	3	52472.70(2)	126.4(3)	3.4(2)	t
B1736–29	1739–2903	1	46965(1)	3.3(2)	1.7(1.0)	t, also in Shemar & Lyne (1996)
B1737–30	1740–3015	1	46991(19)	421(4)	3.4(2)	t, also in McKenna & Lyne (1990), Zou et al. (2008)
B1737–30	1740–3015	2	47289(7)	31(5)	11(12)	t, also in McKenna & Lyne (1990), Zou et al. (2008)
B1737–30	1740–3015	3	47337(27)	7(4)	3(12)	t, also in McKenna & Lyne (1990), Zou et al. (2008)
B1737–30	1740–3015	4	47466(8)	26(2)	0(3)	t, also in McKenna & Lyne (1990), Zou et al. (2008)
B1737–30	1740–3015	5	47670.22(1)	600(1)	3(1)	t, also in McKenna & Lyne (1990), Zou et al. (2008)
B1737–30	1740–3015	6	48158(1)	10(1)	12(2)	t
B1737–30	1740–3015	7	48191.691(4)	659(7)	57(13)	t, also in Shemar & Lyne (1996), Zou et al. (2008)
B1737–30	1740–3015	8	48218(2)	48(10)	8(12)	t, also in Shemar & Lyne (1996), Zou et al. (2008)
B1737–30	1740–3015	9	48431.3(4)	16(2)	3(2)	t, also in Shemar & Lyne (1996), Zou et al. (2008)
B1737–30	1740–3015	10	49047.5(5)	17(1)	2(1)	t, also in Shemar & Lyne (1996), Zou et al. (2008)
B1737–30	1740–3015	11	49239.07(2)	169.7(2)	1.3(2)	t, also in Shemar & Lyne (1996), Zou et al. (2008)
B1737–30	1740–3015	12	49459(2)	10(1)	2(1)	t, also in Krawczyk et al. (2003), Zou et al. (2008)
B1737–30	1740–3015	13	49542.3(1)	6(1)	1(1)	t, also in Krawczyk et al. (2003), Zou et al. (2008)
B1737–30	1740–3015	14	50574.83(1)	442.5(3)	2.4(1)	t, also in Krawczyk et al. (2003), Zou et al. (2008)
B1737–30	1740–3015	15	50939(6)	1444(1)	1.8(1)	t, also in Krawczyk et al. (2003), Urama (2002),
B1737–30	1740–3015	16	51685(21)	0.7(4)	0.1(1)	Janssen & Stappers (2006)
B1737–30	1740–3015	17	51827(2)	0.9(3)	0.1(2)	t, also in Janssen & Stappers (2006)
B1737–30	1740–3015	18	52048(9)	2(3)	1(2)	t, also in Janssen & Stappers (2006)
B1737–30	1740–3015	19	52245(2)	4(1)	–1(2)	t, also in Janssen & Stappers (2006), Zou et al. (2008)
B1737–30	1740–3015	20	52266.0(2)	16(1)	–3(1)	t, also in Janssen & Stappers (2006), Zou et al. (2008)
B1737–30	1740–3015	21	52346.6(1)	158.0(4)	1(1)	t, also in Janssen & Stappers (2006), Zou et al. (2008)
B1737–30	1740–3015	22	52576(3)	0.9(2)	–0.1(1)	t, also in Janssen & Stappers (2006)
B1737–30	1740–3015	23	52779.7(4)	1.7(2)	–0.1(2)	t, also in Janssen & Stappers (2006)
B1737–30	1740–3015	24	52858.78(3)	18.6(3)	1.4(4)	t, also in Janssen & Stappers (2006), Zou et al. (2008)
B1737–30	1740–3015	25	52942.5(1)	20.2(2)	1.5(3)	t, also in Janssen & Stappers (2006), Zou et al. (2008)
B1737–30	1740–3015	26	53023.5190(4)	1850.9(3)	2.4(4)	t, also in Zou et al. (2008)
B1737–30	1740–3015	27	53473.56(1)	0.8(2)	0.2(2)	t
B1737–30	1740–3015	28	54450.19(1)	45.9(3)	4(1)	t
B1737–30	1740–3015	29	54695.19(2)	3.0(2)	1	t
B1737–30	1740–3015	30	54810.9(1)	5.2(3)	1	t
B1737–30	1740–3015	31	54928.6(1)	2.3(2)	1	t
J1737–3137	1737–3137	1	51559(2)	4(1)	0(1)	t
J1737–3137	1737–3137	2	53040(12)	234(1)	2.9(2)	t
J1737–3137	1737–3137	3	54348(4)	1342.4(2)	1.4(2)	t
B1740–31	1743–3150	1	49572(1)	2.2(4)	2(1)	t
J1740+1000	1740+1000	1	54747.6(1)	1.2(4)	1(1)	t
B1757–24	1801–2451	1	49475.95(3)	1987.9(3)	4.6(1)	t, also in Wang et al. (2000)
B1757–24	1801–2451	2	50651.44(3)	1247.4(3)	4.7(2)	t, also in Wang et al. (2000)
B1757–24	1801–2451	3	52054.74(7)	3755.8(4)	6.8(1)	t
B1757–24	1801–2451	4	53033.25(2)	17.4(2)	1.4(1)	t
B1757–24	1801–2451	5	54661(2)	3101(1)	9.3(1)	t
B1758–03	1801–0357	1	48000(1)	3.1(1)	2(2)	t, also in Krawczyk et al. (2003)
B1758–23	1801–2304	1	46907(21)	216.3(2)	–0.5(1)	t, also in Kaspi et al. (1993)
B1758–23	1801–2304	2	47855(24)	230.7(3)	–0.3(2)	t, also in Kaspi et al. (1993)
B1758–23	1801–2304	3	48453.95(4)	348(1)	0(2)	t, also in Wang et al. (2000)
B1758–23	1801–2304	4	49701.7(3)	66(2)	2(2)	t, also in Wang et al. (2000)
B1758–23	1801–2304	5	50055.3(5)	22(1)	–2(1)	t, also in Krawczyk et al. (2003)
B1758–23	1801–2304	6	50363.06(2)	81(1)	2(2)	t, also in Krawczyk et al. (2003)
B1758–23	1801–2304	7	50939(6)	6(3)	4(5)	t
B1758–23	1801–2304	8	52093(26)	646.7(2)	0.9(2)	t
B1758–23	1801–2304	9	53306.98(1)	497(1)	–1(1)	t

... continued on next page

Table 1 – continued

Name	J-name	No. Glt's	MJD days	$\Delta\nu/\nu$ 10^{-9}	$\Delta\dot{\nu}/\dot{\nu}$ 10^{-3}	References
B1800–21	1803–2137	1	48245(11)	4074.4(3)	9.3(1)	t, also in Shemar & Lyne (1996)
B1800–21	1803–2137	2	50264.1(1)	7.1(2)	0.5(1)	t, also in Krawczyk et al. (2003)
B1800–21	1803–2137	3	50777(4)	3183.9(5)	8.0(2)	t, also in Wang et al. (2000)
B1800–21	1803–2137	4	53429(1)	3929.3(4)	10.6(1)	t
J1806–2125	1806–2125	1	51708(123)	15773.1(12.3)	37(3)	t, also in Hobbs et al. (2002)
B1809–173	1812–1718	1	49932(1)	1.5(2)	6(3)	t
B1809–173	1812–1718	2	53106.2(1)	14.8(2)	7(4)	t
B1809–173	1812–1718	3	54365.8(3)	1.4(1)	1(1)	t
J1809–1917	1809–1917	1	53251(2)	1625.1(3)	7.8(3)	t
J1809–2004	1809–2004	1	54196(25)	2(1)	7(7)	t
J1814–1744	1814–1744	1	51371(4)	8(4)	–3(1)	t
J1814–1744	1814–1744	2	51678(1)	10(2)	5(3)	t, also in Janssen & Stappers (2006)
J1814–1744	1814–1744	3	52075(7)	34(2)	–5(3)	t, also in Janssen & Stappers (2006)
J1814–1744	1814–1744	4	53241(12)	3(1)	0.7(4)	t, also in Janssen & Stappers (2006)
J1814–1744	1814–1744	5	53756.4(2)	11(2)	8(4)	t
J1819–1458	1819–1458	1	53925.79(4)	725(3)	78(6)	t, also in Lyne et al. (2009)
J1819–1458	1819–1458	2	54176.5(2)	72(1)	36(2)	t, also in Lyne et al. (2009)
B1821–11	1824–1118	1	54306(3)	2877.0(2)	–10(2)	t
B1821–24	1824–2452	1	51980(31)	0.008(1)	0.00(4)	t, also in Cognard & Backer (2004)
B1822–09	1825–0935	1	49942.1(4)	2.8(2)	–2(1)	t, also in Shabanova (1998)
B1822–09	1825–0935	2	50314(2)	1.3(2)	0(1)	t
B1822–09	1825–0935	3	52056(1)	29.8(1)	3.4(2)	t, mentioned in Zou et al. (2004)
B1822–09	1825–0935	4	52810(1)	1.3(4)	–2(3)	t, mentioned in Zou et al. (2004)
B1822–09	1825–0935	5	53734.6(1)	4(1)	–6(5)	t, also in Shabanova (2007)
B1822–09	1825–0935	6	54114.96(3)	121(1)	–4(3)	t
B1823–13	1826–1334	1	46507(29)	2746(1)	1.7(1)	t, also in Shemar & Lyne (1996)
B1823–13	1826–1334	2	49120(11)	2984.6(3)	7.6(1)	t, also in Shemar & Lyne (1996)
B1823–13	1826–1334	3	53206(1)	0.6(3)	–1(1)	t
B1823–13	1826–1334	4	53259(1)	3(1)	–1(1)	t
B1823–13	1826–1334	5	53737(1)	3581(1)	9.6(4)	t
B1830–08	1833–0827	1	47541.3(1)	0.9(1)	–0.1(1)	t
B1830–08	1833–0827	2	48051(4)	1865.6(1)	1.742(1)	t, also in Shemar & Lyne (1996)
J1830–1135	1830–1135	1	52367(6)	2.1(3)	1(1)	t
J1834–0731	1834–0731	1	53479(1)	4.4(4)	0.6(4)	t
J1835–1106	1835–1106	1	52225.8(2)	15.6(4)	2.5(4)	t, also in Zou et al. (2004)
J1837–0559	1837–0559	1	53150(1)	3.2(3)	13(7)	t
J1838–0453	1838–0453	1	52162(213)	9902(381)	7(1)	t
J1838–0453	1838–0453	2	54140(4)	9(1)	–0.1(4)	t
B1838–04	1841–0425	1	53388(10)	578.60(3)	7.72(3)	t
B1841–05	1844–0538	1	47452(1)	1.0(1)	0.9(3)	t
J1841–0524	1841–0524	1	53562(1)	29(1)	1.0(5)	t
J1841–0524	1841–0524	2	54012.88(5)	25(2)	2(1)	t
J1841–0524	1841–0524	3	54503(21)	1032(1)	0.7(3)	t
1E 1841–045	1841–0456	1	52464.00	15170(82)	96(1)	Based on Table 8 in Dib et al. (2008)
1E 1841–045	1841–0456	2	52997.05	2450(47)	–1(1)	Based on Table 8 in Dib et al. (2008)
1E 1841–045	1841–0456	3	53823.97	1390(82)	–7(3)	Based on Table 8 in Dib et al. (2008)
J1844+0034	1844+00	1	51435(3)	0.3(1)	1(2)	t
J1844+0034	1844+00	2	51722.5(4)	5.2(1)	4(3)	t
J1845–0316	1845–0316	1	52128(1)	30(1)	–2(2)	t
J1845–0316	1845–0316	2	54170(34)	71.9(5)	3(2)	t
J1846–0258	1846–0258	1	52210(10)	2.5(2)	0.93(1)	Livingstone et al. (2006)
J1846–0258	1846–0258	2	53883(2)	6200(300)	4.46(2)	Kuiper & Hermsen (2009), Livingstone et al. (2010)
J1847–0130	1847–0130	1	53426(2)	15(2)	–3(2)	t ^d
J1847–0130	1847–0130	2	54784.449(5)	80(2)	6(3)	t
J1851–0029	1851–0029	1	54493(1)	0.9(2)	–3(2)	t
B1853+01	1856+0113	1	54123(1)	11569(1)	22.0(2)	t
B1859+01	1901+0156	1	51318(70)	42.4(1)	0.8(1)	t
B1859+07	1901+0716	1	46860.95(2)	28(1)	119.9(58.3)	t, also in Shemar & Lyne (1996)
B1900+06	1902+0615	1	48653.7(1)	0.41(5)	0.1(3)	t
B1900+06	1902+0615	2	49447(1)	0.3(1)	–0.1(4)	t
B1900+06	1902+0615	3	50316(2)	0.33(5)	0.5(3)	t
B1900+06	1902+0615	4	51136(4)	0.4(1)	–0.4(4)	t
B1900+06	1902+0615	5	54239(1)	0.26(3)	–0.7(4)	t
B1907–03	1910–0309	1	48252(5)	0.5(1)	0(2)	t, also in Krawczyk et al. (2003)
B1907–03	1910–0309	2	49228.2(1)	2.5(1)	2(1)	t, also in Krawczyk et al. (2003)
B1907–03	1910–0309	3	53231.14(1)	2.7(1)	3(2)	t
B1907+00	1909+0007	1	49530(1)	0.4(1)	3(2)	t
B1907+00	1909+0007	2	51224(9)	0.2(1)	2(1)	t
B1907+00	1909+0007	3	53546(2)	0.5(1)	3(2)	t
B1907+03	1910+0358	1	52321(10)	1.3(3)	9(11)	t
J1913+0446	1913+0446	1	53499.7(5)	6.5(2)	1.4(2)	t
J1913+0832	1913+0832	1	54653.908(1)	38(1)	6(3)	t

... continued on next page

Table 1 – *continued*

Name	J-name	No. Glt's	MJD days	$\Delta\nu/\nu$ 10^{-9}	$\Delta\dot{\nu}/\dot{\nu}$ 10^{-3}	References
B1913+10	1915+1009	1	54154(1)	2.7(1)	0.4(3)	t
J1913+1011	1913+1011	1	54431(2)	0.2(2)	0.1(4)	t
B1917+00	1919+0021	1	50176.6(2)	1.9(2)	10(4)	t, also in Krawczyk et al. (2003)
B1923+04	1926+0431	1	51495(1)	0.08(2)	-0.2(1)	t
B1930+22	1932+2220	1	45989(400)	629(9)	--	t
B1930+22	1932+2220	2	46906(85)	4427(7)	--	t
B1930+22	1932+2220	3	50253(4)	4472(1)	12.2(3)	t, also in Krawczyk et al. (2003)
B1935+25	1937+2544	1	52032(9)	0.03(1)	0.1(1)	t
B1951+32	1952+3252	1	51967(9)	2.3(1)	-0.2(1)	Janssen & Stappers (2006)
B1951+32	1952+3252	2	52385(11)	0.7(1)	0.0(1)	Janssen & Stappers (2006)
B1951+32	1952+3252	3	52912(5)	1.3(1)	0.3(1)	Janssen & Stappers (2006)
B1951+32	1952+3252	4	53305(6)	0.5(1)	0.1(1)	Janssen & Stappers (2006)
B1951+32	1952+3252	5	54103.44(3)	5.2(2)	0.0(4)	t
B1953+50	1955+5059	1	46964(2)	0.04(1)	-0.6(1)	t
B1953+50	1955+5059	2	49038(5)	0.021(4)	-0.1(1)	t
J1957+2831	1957+2831	1	52485(3)	0.26(5)	0.6(3)	t
J1957+2831	1957+2831	2	52912(3)	0.13(3)	0.3(2)	t
J1957+2831	1957+2831	3	54692.8(3)	5.8(3)	5(6)	t
J2021+3651	2021+3651	1	52630.07(5)	2587(2)	6.2(2)	Hessels et al. (2004)
J2021+3651	2021+3651	2	54177(25)	745(6)	5.5(1)	t
B2113+14	2116+1414	1	47989(6)	0.26(4)	8(3)	t
B2224+65	2225+6535	1	43072(40)	1707(1)	3(5)	Backus et al. (1982)
B2224+65	2225+6535	2	51900	0.14(3)	-2.9(2)	Janssen & Stappers (2006)
B2224+65	2225+6535	3	52950	0.08(4)	-1.4(2)	Janssen & Stappers (2006)
B2224+65	2225+6535	4	53434(13)	0.2(1)	--	Janssen & Stappers (2006)
J2229+6114	2229+6114	1	53064(3)	1139.3(3)	12.5(1)	t
J2229+6114	2229+6114	2	54110(1)	327(4)	-3(6)	t
J2229+6114	2229+6114	3	54781.54(3)	4.5(2)	0.1(1)	t
B2255+58	2257+5909	1	49488.2(2)	0.75(4)	1.0(3)	t, also in Krawczyk et al. (2003)
1E 2259+586	2301+5852	1	52443.9(2)	4104(28)	1111(71)	Kaspi et al. (2003)
B2334+61	2337+6151	1	53642(13)	20470(1)	23.8(4)	t, also in Yuan et al. (2010)

t: This work

^a 1E 1048.1–5937^b CXO J164710.2–455216^c 1RXS J170849.0–400910^{c1,c2,c3} Published as glitch candidates (Dib et al. 2008)^d found by Gemma. H. Janssen, private communication.

4 RESULTS: A GLITCH DATABASE

This new search for glitches has found 128 new glitches in 63 pulsars, representing an increase of almost 70% in the number of known glitches. Together, previously published glitches and those found by this search constitute the largest glitch database at the time of writing, comprising a total of 315 glitches in 102 pulsars, including 14 glitches in 6 magnetars. The database contains all the glitches known to us at MJD 55000 (June 2009), hence does not include more recently published events such as those in Yuan et al. (2010) and Weltevrede et al. (2010). Epochs, fractional sizes $\Delta\nu/\nu$ and $\Delta\dot{\nu}/\dot{\nu}$, and references for all glitches are listed in Table 1¹, while a histogram of all glitch sizes, highlighting the new ones, is given in Fig. 2.

Most of the new glitches found occurred in the period MJD 50500–55000, as earlier data had already been analysed by Shemar & Lyne (1996) and Krawczyk et al. (2003). However, we have learned to detect and measure smaller glitches (e.g. Janssen & Stappers 2006), making it easier to identify them in early data, where the signal to noise is typically smaller. As a result, 20 small glitches that had not been reported before were found in data prior to MJD 50500. In addition, two relatively large glitches in the pul-

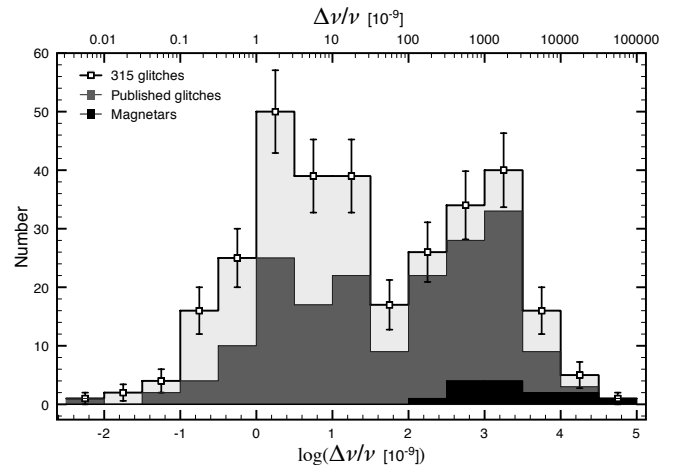


Figure 2. Histogram of the fractional quantity $\Delta\nu/\nu$ for all 315 glitches. The new glitches are included on top of the previously published ones, using a lighter colour, and the contribution of magnetars is plotted using black filling. Errorbars correspond to the square root of the number of event per bin.

sar PSR B1930+22, observed one after the other in 1987, were also measured and included in the database. The reason that they were not reported before is that data prior and between the two events are poor, only allowing measure-

¹ Visit <http://www.jb.man.ac.uk/pulsar/glitches.html> for an online and up-to-date version of Table 1.

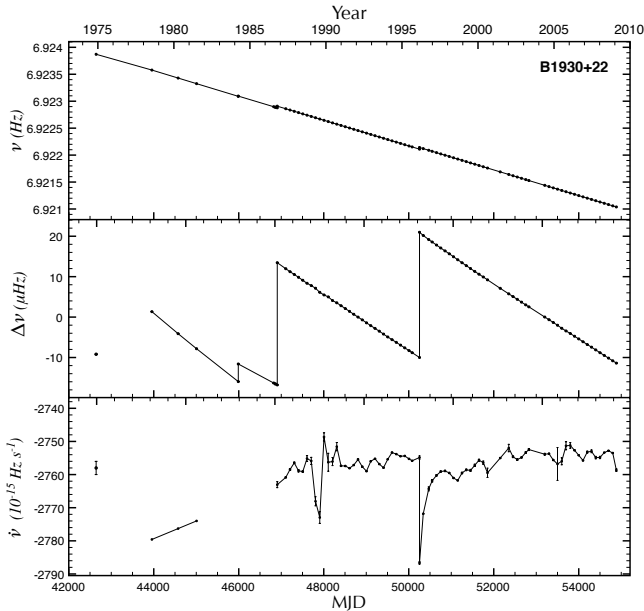


Figure 3. Frequency, frequency residuals and $\dot{\nu}$ evolution of PSR B1930+22 during the last 30 years. Frequency residuals are obtained by removing the main slope observed in the top panel. Although there are only a few observations between 1980 and 1987, and $\dot{\nu}$ cannot be properly determined, the first two glitches are evident in the frequency plots. An even earlier glitch may have occurred at the beginning of 1976, as suggested by the earliest datapoint taken from Gullahorn & Rankin (1978) and from comments in the same work.

ments of $\Delta\nu$, but no good measurements of $\Delta\dot{\nu}$. Moreover, Gullahorn & Rankin (1978) reported on observations of this pulsar in the period 1975-1976 and mentioned the loss of coherence in the timing residuals towards February 1976. JBO observations of this pulsar, starting in 1978, show relatively higher frequency and spindown rate, confirming the possible occurrence of a glitch. The plot in Fig 3 shows the measurement by Gullahorn & Rankin (1978), after being corrected to the currently known position of the pulsar, and all JBO data.

During the search, 83 already published glitches were re-analysed, and the values obtained during the process are included in Table 1, with references to the original papers given in the last column. A comparison between published estimates of the glitch frequency fractional sizes and those obtained in this work are shown in Fig. 4. For glitches smaller than $\Delta\nu/\nu = 2 \times 10^{-9}$ there are a few discrepancies in fractional size, but in general there is a good agreement with published data.

4.1 Lower limit on detectability

A lower limit on the detectability of glitch sizes is not simple to determine; it varies from pulsar to pulsar depending upon TOA errors and temporal coverage. However, a rough estimate could be inferred from the whole collection of detected glitches. The accuracy of glitch size measurements seems poor below $\Delta\nu/\nu \sim 10^{-8}$, as can be seen in Fig. 4, where the comparison with published measurements is plotted. Nonetheless, the contribution of this work to the total

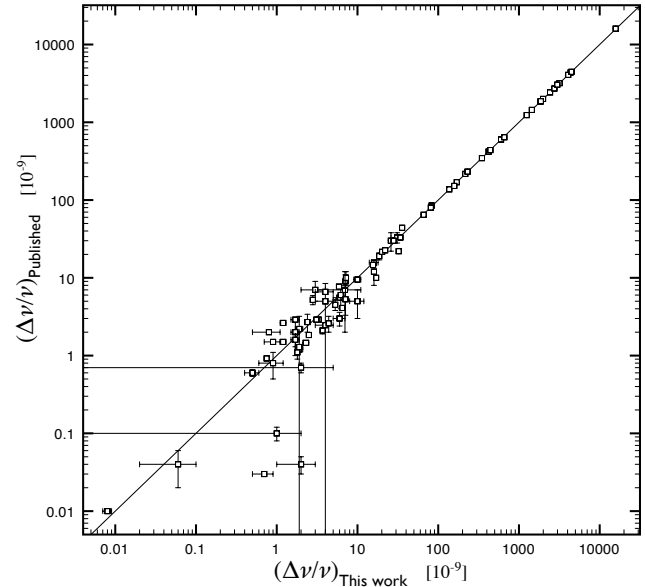


Figure 4. Plot comparing the fractional frequency changes ($\Delta\nu/\nu$) of the 83 glitches re-measured in the course of this work with previously published values. The straight line is $y = x$, indicating the position of equal estimations.

number of small glitches is significant between 10^{-10} and 10^{-8} , suggesting that, even though their parameters may be poorly constrained, most glitches of similar size have been detected.

The analysis presented in the following sections do not depend strongly on the completeness of the sample towards small glitches.

4.2 Visualisation of the new glitches

Plots showing all new glitches are shown in Figs. 5, 6, and 7. For glitches with $\Delta\nu/\nu \gtrsim 30 \times 10^{-9}$ double-panelled plots are presented in Figs. 5 and 6, showing at the top the frequency residuals relative to a simple one-derivative slowdown model fitted to pre glitch data, and the evolution of $\dot{\nu}$ through the glitch at the bottom. The first two glitches seen from PSR B1930+22 are shown separately in Fig. 3.

Fig. 7 shows the timing residuals of all glitches with $\Delta\nu/\nu \lesssim 30 \times 10^{-9}$. For small glitches we only show the timing residuals relative to a slowdown model using a maximum of two frequency derivatives fitted only to pre glitch data. For all plots the horizontal axis has been set such that the origin corresponds to the estimated epoch of the glitch.

5 ANALYSIS

Fig. 8 shows the location in the period-period derivative space (the $P-\dot{P}$ diagram) of every pulsar for which a glitch has been detected. As can be inferred from the diagram, glitches are phenomena which are present in many different populations of neutron stars. Only millisecond pulsars appear not to glitch, with the exception of PSR B1821-24, which has a relatively large \dot{P} and one of the smallest characteristic ages among all millisecond pulsars ($\tau_c = 30$ Myr). In

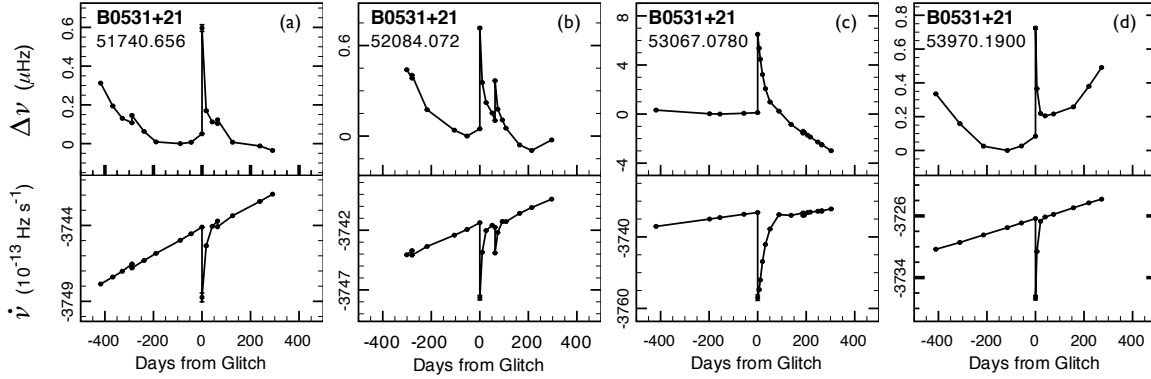


Figure 5. Four of the new largest glitches in the Crab pulsar. Every glitch is shown by plotting the frequency residuals (top) and $\dot{\nu}$ (bottom) against time. The time axis is measured in days and day zero corresponds to the glitch epoch, which is indicated in MJD below the name of the pulsar in each plot.

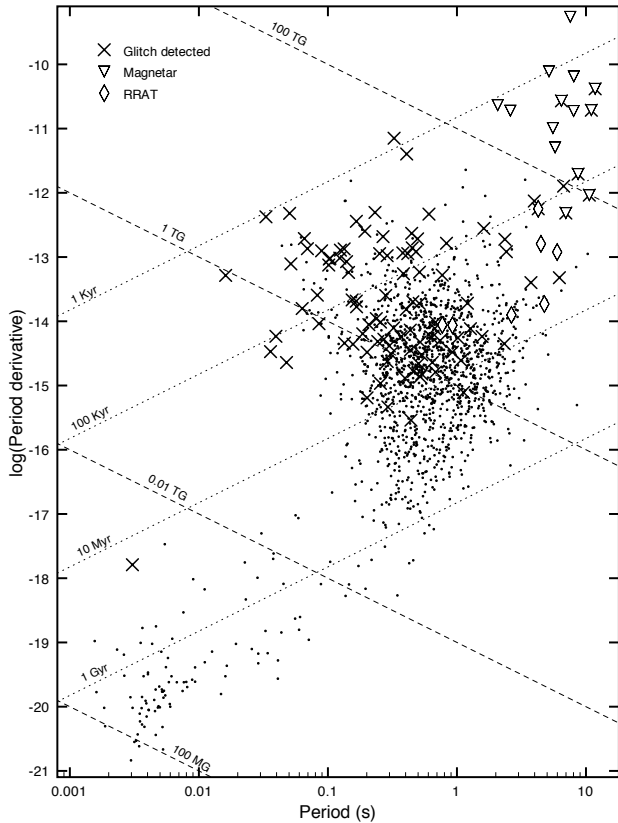


Figure 8. $P-\dot{P}$ diagram showing with the symbol “x” all pulsars that have been seen to glitch. Lines of constant characteristic age and lines of constant magnetic field are shown and labelled.

general, it can be inferred from the figure that most glitching pulsars have a characteristic age τ_c less than ~ 10 Myr.

5.1 Glitching rate and the characteristic age

It has been noted that glitch activity reduces as pulsars age (McKenna & Lyne 1990; Lyne et al. 2000). Fig 9 shows the

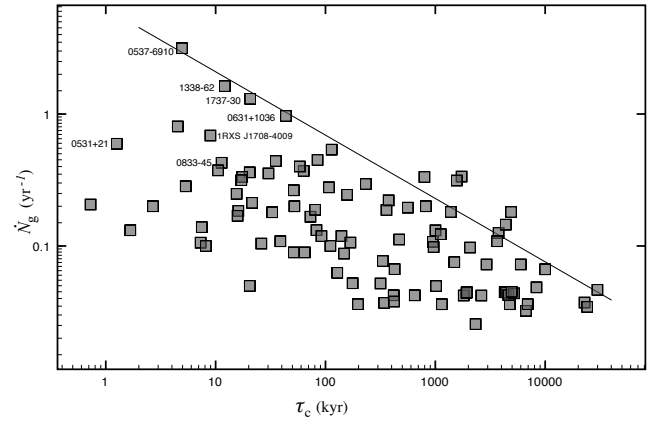


Figure 9. Number of glitches per year \dot{N}_g for individual pulsars versus the characteristic age for all pulsars observed for at least 3 years and with one or more glitch detected. The straight line is a linear fit to the maximum value of \dot{N}_g in each half decade of characteristic age.

number of glitches per year, \dot{N}_g , for all pulsars known to have glitched and which have been observed for at least 3 years, versus their characteristic age. The number of glitches per year was estimated using the whole observation span, when this was known, or the time between the first and last detected glitch, when no other information was available.

The most frequent glitchers, labelled on the plot, appear to coincide with the objects with more detected glitches, showing that the plot is not completely contaminated by objects observed for relatively short time. The observed glitching rate is clearly correlated with τ_c , decreasing for pulsars with larger characteristic ages, confirming the trend seen by McKenna & Lyne (1990) in a much smaller dataset. We note that due to selection effects these data are not complete towards low glitching rates. However, this has no effect over those pulsars with large glitching rates.

The maximum glitching rate, for a given value of τ_c , can be obtained from the envelope defined by the distribution of rates in the plot. To describe the envelope, data were binned

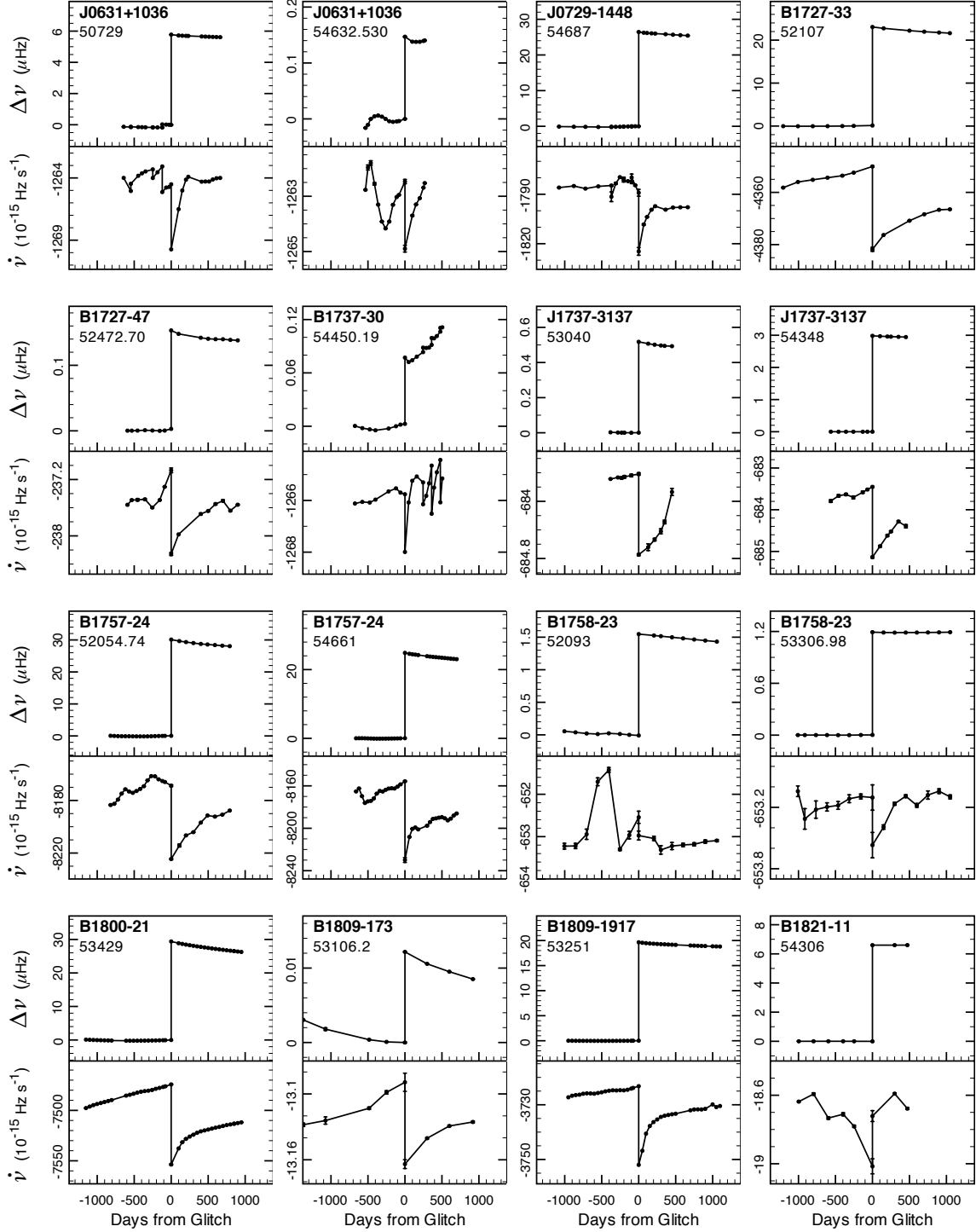


Figure 6. New glitches satisfying $\Delta\nu/\nu \gtrsim 30 \times 10^{-9}$. Every glitch is shown by plotting the frequency residuals relative to a linear model fitted to pre glitch data (top) and $\dot{\nu}$ (bottom) against time. The time axis is measured in days and day zero corresponds to the glitch epoch, which is indicated in MJD below the pulsar name in each plot. There are two glitches in the top left plot for PSR J0631+1036, at MJD 50608.277 and MJD 50729.

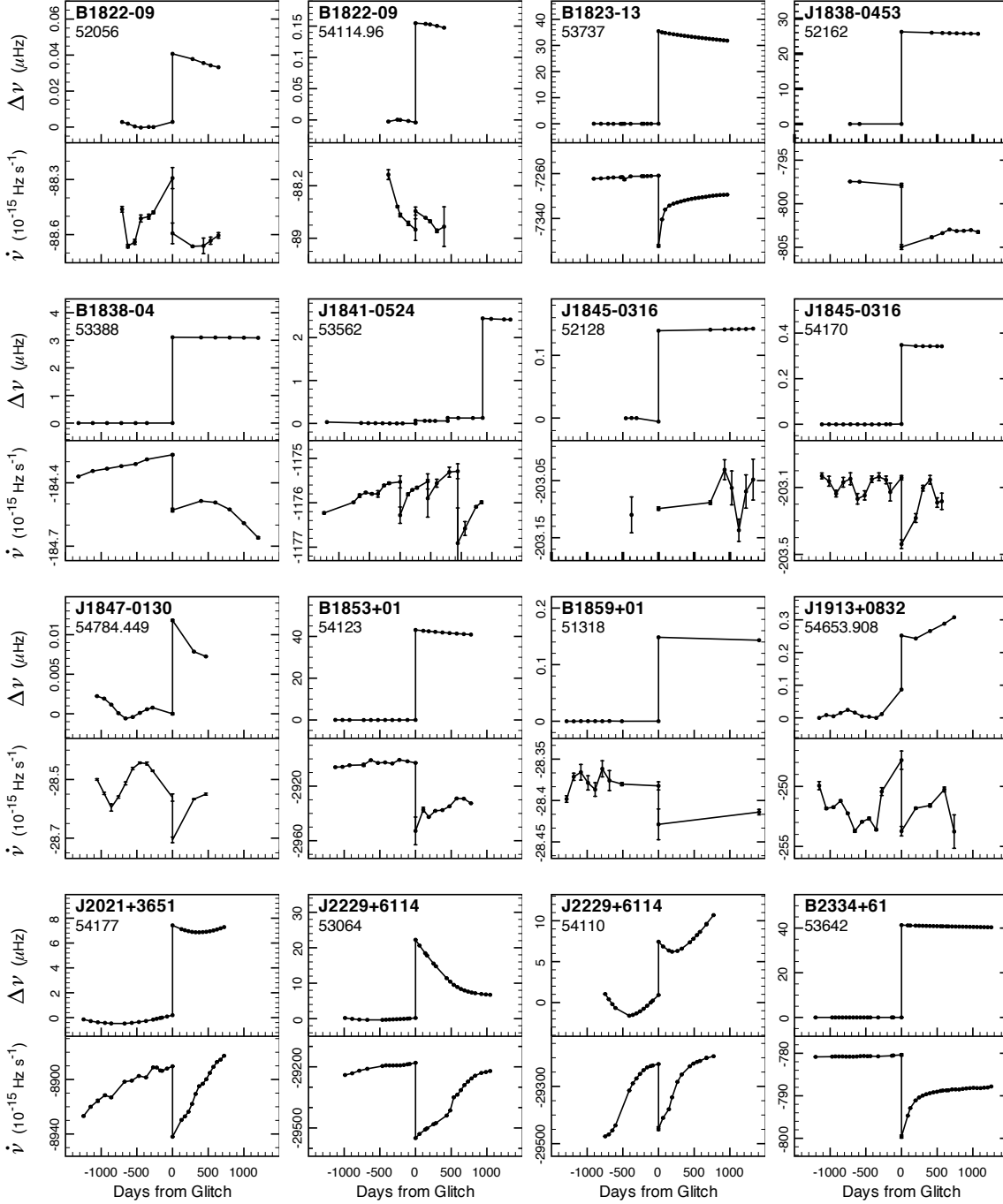


Figure 6 – *continued* There are three glitches in the same plot for PSR J1841–0524, at MJD 53562, MJD 54012.88 and MJD 54503. There is no much data for PSR J1845–0316 around the glitch at MJD 52128, so no good measurements of $\dot{\nu}$ are possible for this epoch. However, the glitch is easily identified in frequency data.

every half decade of characteristic age, and the maximum glitch rate per bin was selected. By fitting a straight line to these selected values the slope of the envelope was obtained, as shown in the plot. The fit indicates that on average, a pulsar with a characteristic age τ_c will glitch a maximum of $(6 \pm 2) \times \tau_c^{-0.48(4)}$ times per year (with τ_c measured in kyr). It should be noted that this simple analysis is directly related to the number of glitches observed, and has nothing to do with the size of the glitches. Accordingly, failing to

detect small glitches could affect these results. The effect of glitch sizes and their frequency are better studied by the integrated glitch activity, which is introduced in the next section.

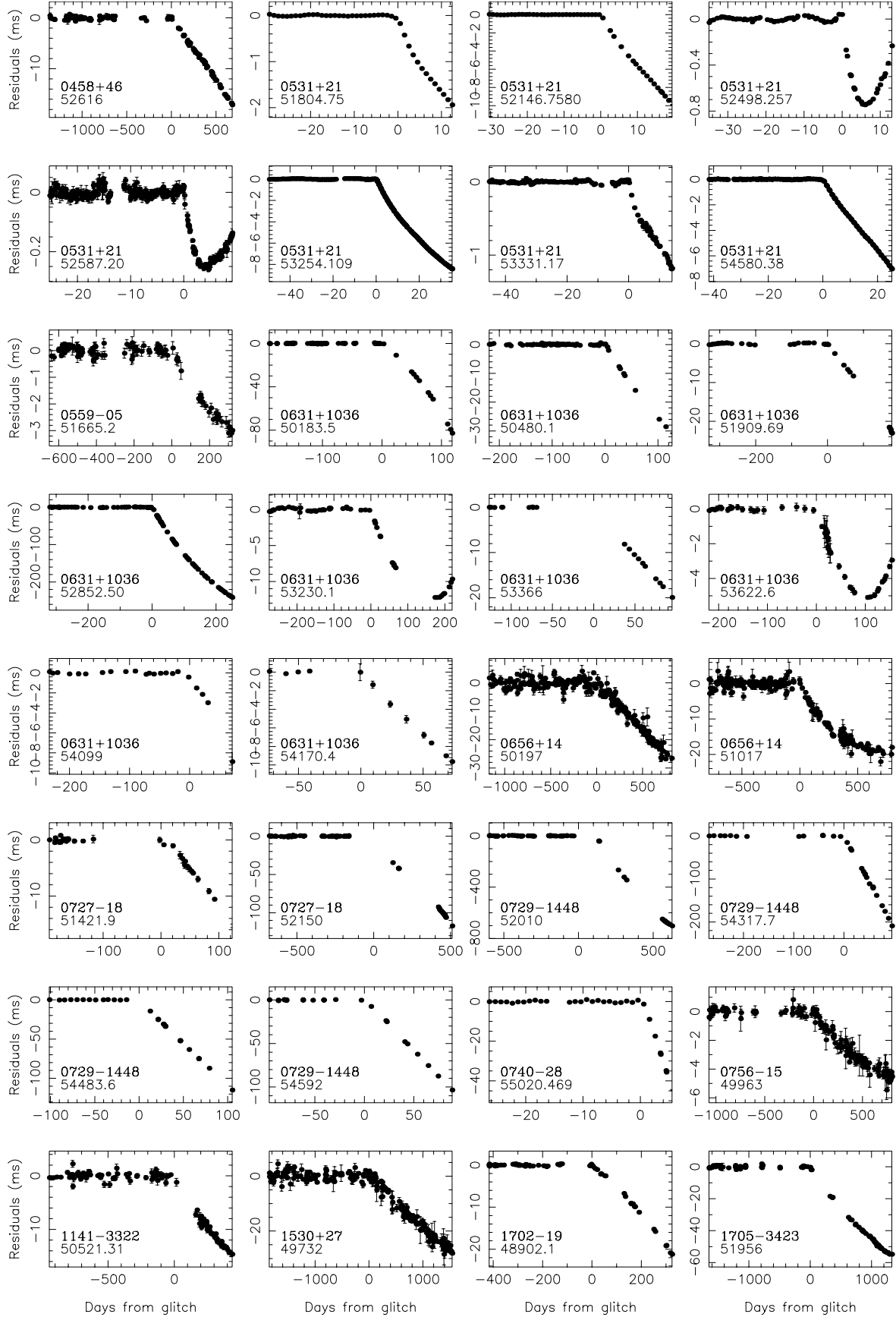


Figure 7. Phase residuals (measured in milliseconds) showing different glitches in several pulsars. The time axis is measured in days and day zero corresponds to the glitch epoch, which is indicated in MJD below the pulsar name in each plot.

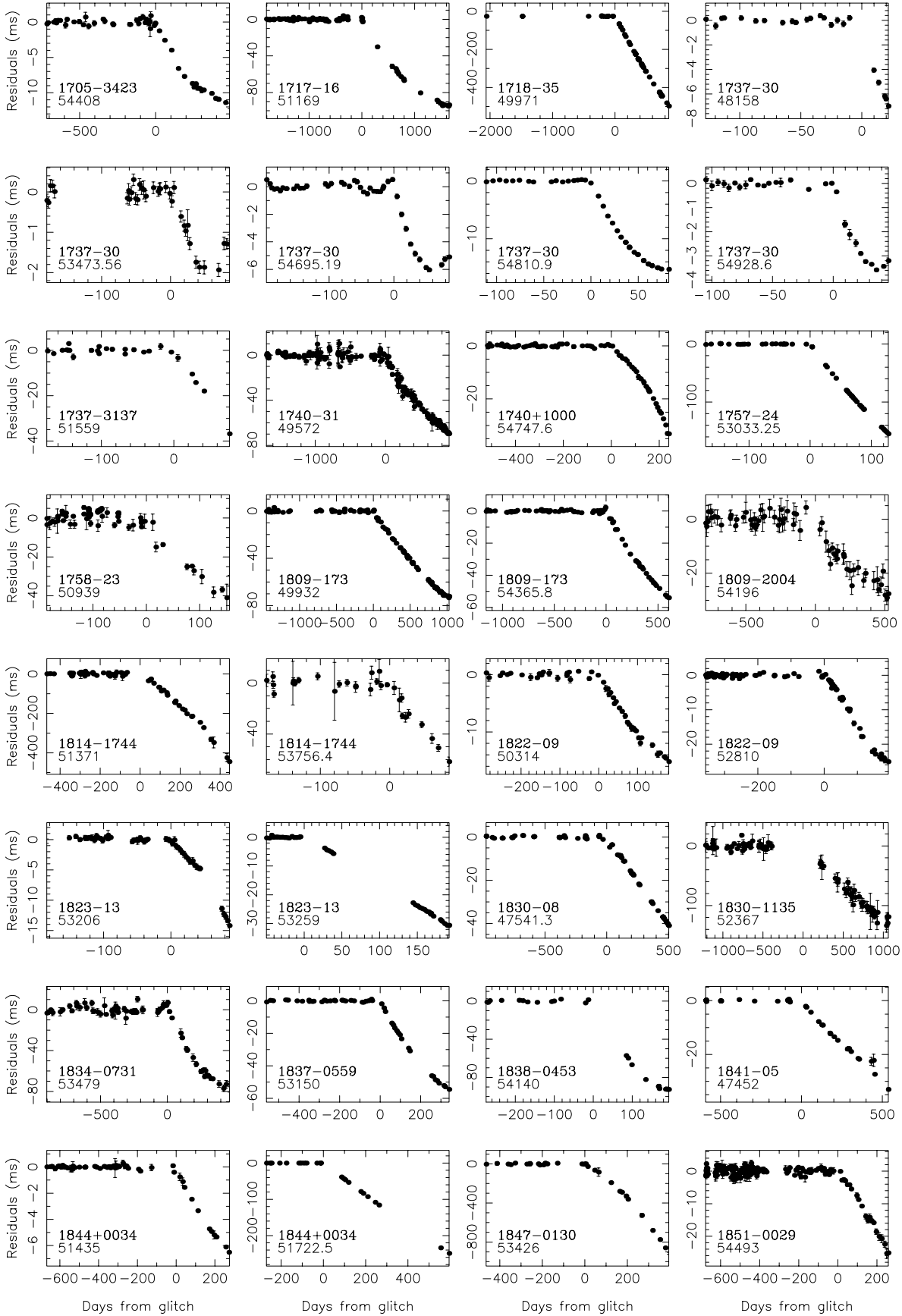


Figure 7 – continued

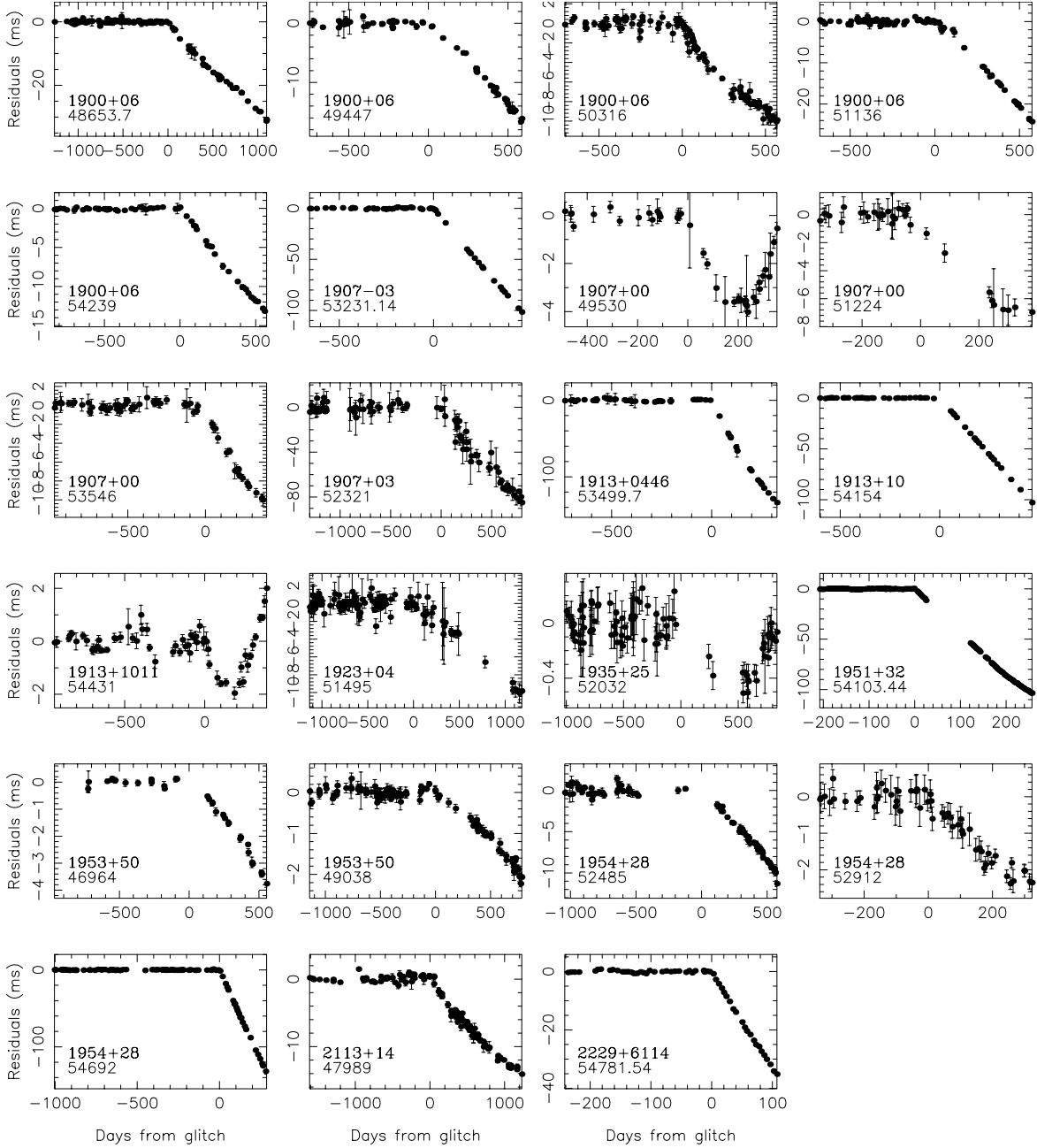


Figure 7 – continued

5.2 Integrated glitch activity

The cumulative effect of spin-up due to glitches on pulsars, measured over several years, can be used to study the glitch activity and its relationship with other parameters. To increase the statistical power, in its estimation we consider a large number of pulsars, including those that have not yet been seen to glitch. Following Lyne et al. (2000), the glitch spin-up rate of a group of pulsars is defined as

$$\dot{\nu}_{\text{glitch}} = \frac{\sum_i \sum_j \Delta \nu_{ij}}{\sum_i T_i}, \quad (2)$$

where the double sum runs over every frequency jump $\Delta \nu_{ij}$ due to the glitch j on the pulsar i , and the sum in the

denominator is the accumulated years of observation of all the pulsars of the group. To calculate the accumulated total time of observation of different groups of pulsars we use a sample of 622 pulsars that have been observed for more than 3 yr at JBO (Table 3) plus all pulsars that have glitched and are not observed at JBO (Table 2).

In Lyne et al. (2000) pulsars were grouped according to their value of $\dot{\nu}$; each group covering a semi-decade of frequency derivative. In Table 4 we have reproduced the same result using the new glitch database and a larger sample of pulsars. The first column contains to the logarithm of the average spindown rate of all pulsars in each semi-decade of frequency derivative. The second column is the total observing

Table 3. J-names and MJD ranges of all pulsars observed at JBO with a span greater than 3 years.

J-name	Range (MJD)	J-name	Range (MJD)	J-name	Range (MJD)	J-name	Range (MJD)
J0014+4746	45120 54945	J0754+3231	44816 54947	J1703-3241	47389 54942	J1801-2451	47553 54945
J0026+6320	53249 54945	J0758-1528	47133 54939	J1705-1906	43587 54935	J1758-2846	52827 54926
J0034-0721	44984 54942	J0814+7429	45277 54940	J1705-3423	49086 54936	J1801-0357	46719 54935
J0034-0534	48763 54939	J0820-1350	45118 54947	J1709-1640	41332 54935	J1758-1931	52586 54946
J0040+5716	46715 54945	J0823+0159	44816 54947	J1708-3426	49086 54935	J1801-2304	46694 54946
J0048+3412	46715 54945	J0826+2637	40264 54949	J1711-1509	47161 54935	J1801-2920	49409 54947
J0055+5117	46715 54945	J0828-3417	43584 54948	J1713+0747	49987 54940	J1758+3030	49872 54945
J0056+4756	46720 54945	J0837+0610	44808 54947	J1717-3425	47880 54936	J1759-2922	49086 54947
J0102+6537	46715 54945	J0849+8028	46715 54946	J1720-1633	46718 54945	J1759-2549	50758 54945
J0108+6608	47387 54945	J0846-3533	44819 54948	J1720-2933	45117 54942	J1803-2137	46270 54948
J0108+6905	46715 54945	J0855-3331	44818 54948	J1720-0212	46237 54935	J1803-2712	47903 54947
J0108-1431	49091 54942	J0900-3144	52616 54944	J1721-1936	48209 54945	J1801-1417	52571 54946
J0117+5914	46715 54946	J0908-1739	44815 54947	J1722-3207	47161 54945	J1801-2154	52586 54940
J0134-2937	49034 54938	J0921+6254	46715 54941	J1721-3532	47907 54934	J1805+0306	47239 54942
J0139+5814	44815 54946	J0922+0638	43587 54947	J1728-0007	47580 54945	J1804-0735	47972 54942
J0137+1654	52754 54945	J0927+23	50059 54381	J1726-3530	50682 54946	J1802-1745	51510 52677
J0141+6009	45109 54946	J0943+1631	43955 54941	J1730-3350	47880 54946	J1807-0847	43871 54942
J0147+5922	46715 54946	J0944-1354	43594 54942	J1733-2228	44817 54945	J1806-1154	48766 54948
J0151-0635	46241 54942	J0946+0951	45278 54947	J1730-2304	49057 54945	J1803-1857	51243 52676
J0152-1637	43834 54942	J0943+22	50110 54941	J1734-0212	46784 54944	J1804-2717	49455 54948
J0156+3949	46785 54945	J0947+27	50059 54941	J1735-0724	47157 54944	J1807-2715	47156 54948
J0157+6212	44818 54949	J0953+0755	40105 54947	J1732-1930	49796 54945	J1805-1504	52599 54946
J0205+6449	52327 54947	J1012-2337	43954 54947	J1734-2415	52828 54931	J1808-2057	46450 54945
J0215+6218	50065 54949	J1012+5307	49221 54941	J1734-3333	50686 54948	J1805-2032	50823 54940
J0218+4232	49092 54949	J1018-1642	46716 54948	J1737-3555	47880 49367	J1806-2125	50802 54940
J0231+7026	46715 54945	J1022+1001	49831 54947	J1738-3211	46564 54947	J1809-2109	46564 54934
J0304+1932	45943 54949	J1024-0719	49417 54947	J1735-3258	50760 54946	J1807+0756	50173 54940
J0323+3944	44997 54949	J1034-3224	48775 54948	J1736-2457	52718 54931	J1807-2459A	51700 54947
J0332+5434	45119 54946	J1041-1942	44815 54948	J1736-2843	51410 54946	J1808-2701	52751 54931
J0335+4555	46717 54949	J1047-3032	49419 54948	J1739-2903	46270 54947	J1808-0813	49071 54948
J0343+5312	44815 54946	J1115+5030	46060 54941	J1739-3131	46270 54947	J1808+00	49872 54948
J0343+5312	44815 47562	J1136+1551	40159 54946	J1736+05	49872 54944	J1808-1726	52718 54946
J0357+5236	46717 54949	J1141-3107	49071 54948	J1737-3137	50759 54925	J1808-3249	52589 54932
J0358+5413	41808 54946	J1141-3322	49420 54940	J1740+1311	43871 54935	J1808-1020	52599 54931
J0406+6138	43956 54949	J1239+2453	40443 54946	J1740-3015	46270 54947	J1812-1718	46271 54936
J0407+1607	52719 54949	J1238+21	50173 54942	J1737-3102	50759 54946	J1812-1733	47904 54945
J0415+6954	46717 54945	J1246+22	49219 54942	J1741-0840	44815 54935	J1809-1917	50821 54939
J0417+35	50069 54938	J1257-1027	46716 54946	J1738-2330	52772 54931	J1809-2004	51510 54945
J0421-0345	52922 54942	J1300+1240	48138 54946	J1738-2955	50787 54946	J1812+0226	47207 54936
J0435+27	50173 54939	J1311-1228	46716 54946	J1739-3023	50728 54946	J1810-2005	50758 54939
J0450-1248	44817 54948	J1321+8323	45120 54946	J1743-0339	43584 54935	J1811+0702	50070 54936
J0448-2749	49383 54948	J1332-3032	49421 54946	J1743-1351	46784 54929	J1811-2439	52859 54931
J0452-1759	45118 54948	J1358-2533	48777 54942	J1743-3150	47880 54926	J1813+4013	47155 54945
J0454+5543	47203 54945	J1455-3330	48921 54946	J1741+2758	50028 54945	J1811-1736	50803 54945
J0502+4654	46238 54946	J1509+5531	44937 54946	J1740-3052	50761 54925	J1812-1910	51250 54945
J0459-0210	49071 54948	J1518+4904	49798 54946	J1745-3040	45118 54926	J1812-2102	50803 54945
J0520-2553	49797 54948	J1532+2745	45109 54946	J1743-3153	50879 54926	J1812-2526	52871 54931
J0525+1115	43955 54948	J1537+1155	48140 54942	J1744-3130	50761 54926	J1816-1729	46271 54934
J0528+2200	45010 54947	J1543-0620	46237 54940	J1744-2335	49086 54934	J1816-2650	44818 54934
J0534+2200	43954 54947	J1543+0929	44814 54945	J1744-1134	49534 54933	J1814-0618	52718 54948
J0538+2817	50245 54949	J1549+2113	52732 54942	J1748-2446A	47952 54934	J1814-1744	50833 54945
J0543+2329	45118 54946	J1555-2341	47137 54933	J1748-2444	48327 54934	J1817-2311	45219 54381
J0540+32	53549 54947	J1555-3134	47132 54933	J1748-2446C	50452 54935	J1818-1422	46271 54934
J0601-0527	44815 54948	J1603-2712	47137 54933	J1748-1300	47158 54935	J1815-1910	50722 54940
J0611+30	50024 54947	J1603-2531	48777 54933	J1748-2021	47882 54941	J1816-0755	52599 54948
J0609+2130	52757 54948	J1607-0032	41331 54940	J1746-2856	53623 54941	J1820-1346	46271 54936
J0612+3721	46715 54947	J1610-1322	46718 54940	J1749-3002	47896 54935	J1820-1818	47904 54934
J0614+2229	45082 54947	J1614+0737	47139 54948	J1747-2958	52307 54376	J1820-0427	40614 54936
J0613-0200	49031 54947	J1615-2940	43954 54933	J1750-3157	47881 54935	J1818-1541	51243 54939
J0621+1002	49965 54948	J1623-0908	44815 54941	J1752-2806	40352 54935	J1820-0509	52608 54948
J0624-0424	44815 54948	J1623-2631	47082 54941	J1750-3503	48777 54935	J1819-1408	51244 52676
J0625+10	49872 54944	J1627+1419	50181 54375	J1753-2501	46565 54935	J1822-2256	44819 54934
J0629+2415	46241 54947	J1635+2418	44819 54945	J1751-3323	51832 54926	J1823-1115	47475 54939
J0630-2834	45195 54948	J1640+2224	50023 54946	J1751-2857	51973 54946	J1822-1400	46302 54936
J0631+1036	49994 54942	J1645-0317	40486 54940	J1753-1914	52828 54931	J1820-1529	51245 54939
J0653+8051	44817 54946	J1643-1224	49057 54940	J1756-2435	46564 54945	J1823-3021A	48269 54944
J0700+6418	44816 54946	J1645+1012	50181 54941	J1754+5201	46722 54946	J1823-3021B	47978 54934
J0659+1414	43955 54949	J1648-3256	49086 54945	J1757-2421	43589 54945	J1823-3106	44325 54936
J0725-1635	52882 54949	J1651-1709	47389 54942	J1754-3510	52718 54932	J1821-0256	52732 54948
J0726-2612	52773 54942	J1652-2404	44818 54942	J1755-1650	52860 54931	J1823+0550	44815 54924
J0729-1836	43584 54949	J1649+2533	50028 54946	J1755-2521	51243 54945	J1824-1118	46612 54936
J0737-2202	50832 54948	J1650-1654	49071 54942	J1755-25211	51811 54945	J1821+1715	50173 54928
J0737-3039A	52856 54940	J1652+2651	50028 54946	J1755-2534	51245 54945	J1824-1945	44817 54934
J0737-3039B	52971 54948	J1654-2713	49383 54942	J1759-2205	46781 54945	J1824-2452	47054 54934
J0738-4042	51895 54224	J1659-1305	46718 54942	J1756-2225	51218 54945	J1825+0004	46785 54947
J0742-2822	44838 54949	J1700-3312	49086 54946	J1756-2251	52810 54944	J1822+0705	50028 54936
J0751+1807	49343 54947	J1703-1846	47157 54935	J1800-2343	47207 51461	J1822-0848	52749 54939

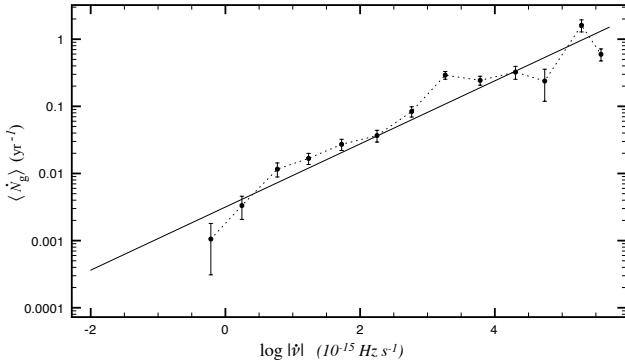
... continued on next page

Table 3 – *continued*

J-name	Range (MJD)		J-name	Range (MJD)		J-name	Range (MJD)		J-name	Range (MJD)	
J1825–0935	45008	54948	J1844+00	49872	54936	J1906+0746	53511	54947	J1952+1410	46727	54938
J1822–1252	51242	54945	J1844–0310	51510	54946	J1907+0918	51274	54939	J1950+05	49873	54937
J1825–1446	46302	54939	J1847–0402	44816	54936	J1909+0007	44818	54936	J1952+3252	47029	54945
J1823–0154	49086	54947	J1845–0826	52752	54931	J1909+0254	44816	54936	J1954+2923	44808	54938
J1826–1131	46270	54939	J1845–1351	52749	54931	J1910–0309	44817	54938	J1955+2908	45471	54938
J1826–1334	46302	54944	J1843–1507	52718	54931	J1910+0358	47389	54936	J1955+5059	43960	54938
J1824–0127	52608	54932	J1848–0123	47388	54936	J1907+0345	51643	54929	J1957+2831	50239	54938
J1827–0958	46302	54939	J1845–0316	51609	54942	J1909+1102	44816	54938	J2002+3217	46564	54948
J1824–2233	52859	54932	J1845+0623	52718	54932	J1910+1231	44820	54938	J2002+4050	46717	54942
J1824–2328	52751	54932	J1845–0743	51833	54940	J1908+0839	51251	54944	J2002+30	49872	54940
J1824–1423	51508	52676	J1845–1114	52599	54931	J1908+0909	51139	54933	J2004+3137	44817	54946
J1826–1526	51510	52619	J1848–1952	44817	54936	J1909+0912	51252	54929	J2006–0807	43591	54941
J1829–1751	44818	54939	J1847–0605	51508	52621	J1909+0616	51509	54930	J2005–0020	49384	54941
J1827–0750	52974	54931	J1849–0636	44817	54936	J1909+0751	53693	54944	J2006+3104	53630	54949
J1828–2119	52599	54931	J1846–0749	52871	54932	J1910+0534	51508	52620	J2010+2845	53630	54949
J1830–1059	46612	54944	J1847–0130	52135	54942	J1910+1256	52871	54948	J2013+3845	46718	54946
J1828–1101	51243	54939	J1848–1150	52608	54931	J1912+2104	44817	54931	J2018+2839	45121	54938
J1828–1057	51305	54939	J1851+0418	46785	54925	J1913–0440	40653	54936	J2018+34	53550	54946
J1829+0000	52752	54932	J1848–0601	52609	54932	J1911–1114	49605	54948	J2019+2425	49258	54936
J1832–0827	46271	54939	J1848+0604	52733	54924	J1914+1122	44820	54938	J2022+2854	45108	54938
J1832–1021	46271	54939	J1848+12	46723	54927	J1913+1400	47158	54938	J2021+3651	52590	54948
J1830–0131	52718	54948	J1850+1335	46785	54936	J1911+1347	52718	54931	J2022+5154	45118	54946
J1833–0827	46449	54944	J1848–1414	49071	54936	J1913+0832	51643	54939	J2023+5037	46785	54946
J1830–1135	51816	54945	J1852+0031	46564	54936	J1913+0446	51832	54939	J2029+3744	46716	54941
J1834–0010	46785	54381	J1849+0127	51302	54948	J1913+0904	53004	54948	J2030+2228	43587	54936
J1833–0338	46782	54936	J1849+0409	52608	54932	J1913+1000	52602	54929	J2033+17	50023	54944
J1834–0426	44814	54936	J1849–0317	51510	54946	J1913+1011	51465	54935	J2037+3621	46720	54946
J1831–0952	51302	54939	J1851–0114	52599	54932	J1915+1009	45279	54948	J2038+5319	47388	54946
J1831–1223	51478	52620	J1851+0118	52614	54948	J1913+1145	51138	54925	J2040+1657	52751	54934
J1831–1329	51250	54945	J1854–1421	45194	54936	J1915+1606	46671	54929	J2043+2740	50256	54947
J1832+0029	52887	54947	J1851–0029	53817	54948	J1915+1647	45117	54930	J2046–0421	44819	54941
J1835–0643	46564	54936	J1854+1050	46724	54938	J1914+0219	52608	54948	J2046+1540	43587	54932
J1832–0644	51251	54939	J1852–2610	48777	54936	J1916+0951	43587	54887	J2048–1616	44818	54940
J1833–0559	51510	54945	J1853–0004	52280	54944	J1916+1312	47157	54937	J2046+5708	46783	54946
J1836–0436	46449	54936	J1853+0056	51250	54948	J1915+0227	52599	54948	J2051–0827	49535	54941
J1834–0602	51477	52677	J1856+0113	47577	54948	J1917+1353	45108	54947	J2055+2209	46718	54940
J1837–0653	46270	54936	J1853+0505	51817	54948	J1917+2224	46716	54932	J2055+3630	46057	54941
J1834–0731	51833	54945	J1853+0545	51634	54948	J1918+1444	45108	54945	J2108+4441	44817	54946
J1834–0742	51670	54945	J1853+1303	53044	54939	J1916+0748	50173	54930	J2108–3429	49796	54436
J1836–1008	46951	54936	J1857+0057	46727	54938	J1919+0021	46001	54948	J2113+2754	44817	54949
J1834+10	49872	54936	J1855+0206	53630	54944	J1921+1948	44816	54940	J2113+4644	44326	54937
J1834–1855	52744	54931	J1857+0212	46447	54944	J1920+2650	46718	54937	J2116+1414	44329	54934
J1834–0031	52599	54932	J1857+0943	46462	54938	J1919+1315	53630	54925	J2124+1407	47131	54934
J1835–0924	51510	54940	J1856–0526	52718	54931	J1921+1419	43587	54929	J2124–3358	49142	54940
J1835–0944	53525	54932	J1859+00	49873	54936	J1921+2153	45118	54937	J2139+00	49873	54934
J1835–1020	51250	54940	J1857+0143	52407	54947	J1920+1110	51508	52650	J2145–0750	48918	54933
J1835–1106	49071	54940	J1858+0215	51510	52621	J1922+2018	44819	54937	J2150+5247	46716	54949
J1836–1324	53072	54931	J1857+0210	51510	54948	J1922+2110	47139	54937	J2149+6329	44818	54949
J1837–0045	49383	54936	J1857+0526	51811	54948	J1921+0812	53083	54932	J2155–3118	44819	54940
J1837–0559	51153	54945	J1900–2600	45121	54938	J1924+2040	45194	54931	J2157+4017	45943	54946
J1837–1243	51250	54948	J1901+0156	46724	54936	J1926+0431	44819	54948	J2212+2933	46716	54939
J1837–0604	51089	54945	J1901+0331	44814	54938	J1926+1434	44820	54937	J2219+4754	45943	54949
J1838–0453	51251	54948	J1901+0716	46564	54938	J1926+1648	47030	54940	J2222+2923	49872	54939
J1841–0425	46270	54936	J1901–0906	49086	54936	J1927+1852	47236	54937	J2225+6535	44817	54948
J1838+1650	52732	54926	J1900–0051	51635	54948	J1927+0911	53153	54944	J2227+30	50024	54946
J1839–0321	51250	54946	J1903+0135	44821	54938	J1928+1746	53552	54936	J2229+6205	44818	54935
J1842–0359	46270	54936	J1902+0556	43587	54938	J1929+00	49872	54941	J2229+2643	49829	54937
J1839–0905	51670	54946	J1902+0615	44817	54938	J1932+1059	40401	54937	J2229+6114	51977	54946
J1841+0912	43871	54936	J1903–0632	47391	54936	J1932+2020	47155	54938	J2235+1506	49219	54946
J1839–1238	52599	54931	J1900+30	49872	54945	J1932+2220	44816	54947	J2242+6950	46717	54937
J1840+5640	44817	54946	J1901+00	49872	54938	J1933+2421	48505	54949	J2248–0101	49072	54946
J1840–0840	52988	54931	J1900+0227	51510	52620	J1931+30	49873	54948	J2257+5909	44817	54935
J1840–1207	52599	54931	J1901+0355	52588	54930	J1937+2544	46786	54937	J2305+3100	44817	54937
J1841+0130	52749	54932	J1901+0413	51811	54929	J1939+2134	45297	54940	J2305+4707	46716	54935
J1841–0345	51508	54939	J1901+0435	52599	54941	J1939+2449	47236	54937	J2308+5547	44817	54935
J1844–0433	46597	54936	J1905–0056	46786	54938	J1941–2602	43584	54934	J2313+4253	43871	54946
J1844–0538	46270	54936	J1903–0258	52718	54932	J1938+0650	50028	54941	J2317+2149	44815	54947
J1841–0524	51816	54939	J1903+0601	51643	54929	J1938+20	53550	54948	J2317+1439	49868	54946
J1841–0157	51670	54946	J1905+0709	46270	54929	J1943–1237	43587	54934	J2321+6024	45197	54935
J1844–0244	46447	54936	J1904+0004	49071	54938	J1941+1341	52599	54935	J2322+2057	49258	54947
J1842+0257	52608	54932	J1904–0150	52752	54932	J1944–1750	43591	54934	J2325+6316	43956	54935
J1842+0358	52732	54932	J1906+0641	46270	54938	J1945–0040	43587	54941	J2326+6113	44817	54932
J1845–0434	52909	54936	J1904+07	53550	54925	J1946–2913	43587	54934	J2330–2005	45111	54946
J1842–0415	51250	54946	J1904+0800	51832	54930	J1946+1805	45118	54938	J2337+6151	46717	54946
J1842–0905	51460	54946	J1903+0925	53050	54948	J1946+2535	53630	54949	J2346–0609	49383	54946
J1844+1454	43584	54926	J1904–1224	49419	54938	J1949–2524	43587	54934	J2354+6155	44817	54946
J1843–0355	51250	54940	J1905+0616	51508	54929	J1946+2611	52586	54939	J2353+2246	49965	54947
J1843–0459	51508	52620	J1905+0400	51492	54929	J1948+3540	44816	54948			
J1843–1113	51895	54946	J1907+4002	44817	54945	J1947+10	49873	54937			

Table 2. Observation time spans (T) of 22 pulsars not observed at JBO that have glitched. There are 6 magnetars among them.

J-name	T (yr)	J-name	T (yr)
J0146+6145 ^a	6	J1341–6220	7.4
J0537–6910	7.3	J1539–5626	3
J0540–6919	7.6	J1614–5048	7.2
J0633+1746	27	J1617–5055	10
J0835–4510	37.5	J1644–4559	16
J1048–5832	8.3	J1647–4552 ^c	0.3
J1048–5937 ^b	12	J1709–4429	3
J1105–6107	5.4	J1708–4009 ^d	8.7
J1123–6259	5	J1841–0456 ^e	3.7
J1302–6350	13	J1846–0258	9.7
J1328–4357	1.3	J2301+5852 ^f	5

^a 4U 0142+61^b 1E 1048.1–5937^c CXO J164710.2–455216^d 1RXS J170849.0–400910^e 1E 1841–045^f 1E 2259+586**Figure 10.** The mean glitch rate $\langle \dot{N}_g \rangle$ versus $|\dot{\nu}|$ (Table 4). The solid line is a linear fit to the data and has the form $\langle \dot{N}_g \rangle \propto |\dot{\nu}|^{0.47(4)}$.

time span T_i of the group in years and the next four columns are the total number of glitches N_g , the mean glitching rate $\langle \dot{N}_g \rangle = N_g / \sum T_i$, the number of pulsars with a glitch detected N_{pg} and the total number of pulsars in the group N_p . The 6th column shows the cumulative effects of the frequency jumps, which when divided by $\sum T_i$ gives the glitch spin-up rate, shown in the last column. Errors for $\langle \dot{N}_g \rangle$ are estimated as $\sqrt{N_g / \sum T_i}$ and the errors for the glitch spin-up rate as $\dot{\nu}_{\text{glitch}} / \sqrt{N_g}$. The new results, plotted in Fig. 11, are perfectly compatible with those obtained by Lyne et al. (2000). Thanks to the larger sample, we have been able to reduce the size of the errorbars significantly, and the $\dot{\nu}$ range for which a slope close to 1 was claimed is now better defined (for $|\dot{\nu}_{-15}|$ between 10 and $\sim 32,000$, where $\dot{\nu}_{-15}$ is $\dot{\nu}$ in units of $10^{-15} \text{ Hz s}^{-1}$). A straight line with a slope of one is included in the plot for comparison. We note that the largest value of the spin-up rate are the result of the high glitch activity of PSR J0537–6910 and the Crab pulsar. Due to the low number of pulsars with very high spindown rate in the sample, these two pulsars dominate completely the integrated glitch activity of the corresponding $\dot{\nu}$ bins (see Table 4).

The low glitch activity of pulsars with small spindown rates is caused by small and rare glitches. There are no glitches detected for pulsars with $|\dot{\nu}_{-15}| < 0.5 \text{ Hz s}^{-1}$. Fig. 10 shows the mean glitching rate $\langle \dot{N}_g \rangle$ against $|\dot{\nu}|$ using data from Table 4. A linear fit to that data gives $\langle \dot{N}_g \rangle \propto |\dot{\nu}|^{0.47(4)}$. This suggests that for the first 3 bins no glitches should be expected for the given accumulated observation times ($\sum T_i$), and only one (1.25) glitch should be expected for the bin centred at $\log(|\dot{\nu}_{-15}|) = -0.73$. Using the same fit, the necessary accumulated time to observe one glitch can be estimated for each bin, and given an assumed glitch size, sensible upper limits for the glitch activity in those $\dot{\nu}$ bins can be estimated. It is important to notice that the bins centred on $\log(|\dot{\nu}_{-15}|)$ values of 0.25 and -0.22 , which present the lowest $\dot{\nu}_{\text{glitch}}$ values, have the longest accumulated observation times and also the largest number of observed pulsars. There is an increase of more than two orders of magnitude of $\dot{\nu}_{\text{glitch}}$ from these bins towards larger spindown rates. This change may imply important differences between objects with lower and higher $\dot{\nu}$ values.

The average glitch size for the pulsars in these two bins is $0.0004 \mu\text{Hz}$, and adding all jumps together the glitch contribution is not larger than $0.004 \mu\text{Hz}$. By using the estimated accumulated time necessary to observe at least one glitch, and assuming a glitch size of $0.0004 \mu\text{Hz}$, the glitch spin-up rate for the 4 bins with lowest spindown rate were estimated and plotted in Fig. 11a using white triangles. In the same manner, the glitch spin-up rate was estimated again, but now assuming that the glitch had a frequency size of $0.03 \mu\text{Hz}$ (which roughly corresponds to the centre of the general $\Delta\nu$ distribution, see § 5.3), and the results are plotted using black triangles. Finally, the glitch activity obtained if a glitch with $\Delta\nu = 1 \mu\text{Hz}$ was detected in the data of pulsars in these 4 bins, using the currently available accumulated observing times, is plotted with a dotted line. As $\sum T_i$ gets shorter towards lower $|\dot{\nu}|$, the maximum spin-up rate estimates grow alike.

In Fig. 11b the percentage of $\dot{\nu}$ reversed by glitch activity is plotted as a function of the slowdown rate. For pulsars with low $|\dot{\nu}|$ values, for which no glitch has been detected, the percentage was calculated using the same glitch spin-up rates estimated for the upper plot. However, only glitch activity corresponding to one glitch with $\Delta\nu = 0.0004 \mu\text{Hz}$ fall below 1%. If estimated for a glitch activity produced by one glitch with a frequency jump of $0.03 \mu\text{Hz}$ the amount of $\dot{\nu}$ reversed by glitch activity rises up to more than 2%, for $\log(|\dot{\nu}|) = 0.018$, and about 25% for the first bin. The fact that the percentage of $\dot{\nu}$ reversed by glitches of those pulsars exhibiting the largest glitch activity is always less than 2%, suggests that low spindown rate objects are likely to present smaller or similar ratios. Consequently, the glitch activity values estimated for one glitch having $\Delta\nu = 0.0004 \mu\text{Hz}$ (white triangles) might represent realistic upper limits.

5.2.1 Glitch spin-up rate and the characteristic age

Following the same procedure, the characteristic age τ_c can be used to divide the sample of pulsars, instead of $\dot{\nu}$. The sample was divided in half decades of τ_c and the results are shown in Table 5 and in Fig. 12. As expected, due to the dependence of the characteristic age on $\dot{\nu}$, the glitch spin-up rate decreases towards large values of τ_c . The curve, similar

Table 4. Mean rates of glitch occurrence, $\langle \dot{N}_g \rangle$, and mean glitch spin-up rates of pulsars grouped every half decade of $|\dot{\nu}|$.

$\log(\dot{\nu})$ ($10^{-15} \text{ Hz s}^{-1}$)	$\sum T_i$ (yr)	N_g	$\langle \dot{N}_g \rangle$ yr^{-1}	N_{pg}	N_p	$\sum \sum \Delta \nu_{ij}$ (μHz)	$\dot{\nu}_{\text{glitch}}$ ($10^{-15} \text{ Hz s}^{-1}$)
-2.03	28	0	0	0	1	0	0
-1.75	48	0	0	0	3	0	0
-1.22	303	0	0	0	18	0	0
-0.73	892	0	0	0	49	0	0
-0.22	1895	2	0.001(1)	2	107	0.0009	0.00001(1)
0.25	2104	7	0.003(1)	5	110	0.003	0.00005(1)
0.77	1552	18	0.012(3)	12	82	0.84	0.017(1)
1.24	1671	28	0.016(3)	16	92	13	0.024(1)
1.73	1031	28	0.027(5)	14	66	17	0.051(2)
2.25	682	25	0.04(1)	10	44	31	1.5(1)
2.77	393	33	0.08(1)	13	28	110	9.1(3)
3.26	199	58	0.29(4)	8	15	180	28.1(5)
3.78	177	43	0.24(4)	12	15	460	83(2)
4.31	65	21	0.3(1)	4	4	380	188(9)
4.74	17	4	0.2(1)	2	2	82	155(40)
5.29	15	24	1.6(3)	2	2	410	873(4)
5.58	40	24	0.6(1)	1	1	15	11.9(5)

to that depending on $\dot{\nu}$, exhibits a change of slope before becoming zero. The maximum spin-up rate is found for pulsars with characteristic ages around 10 kyr and is about $250 \times 10^{-15} \text{ Hz s}^{-1}$. Because in this case PSR J0537–6910 is included together with other pulsars of similar characteristic age, the maximum glitch spin-up rate is about 3 times smaller than the one obtained when grouping pulsars according to their spindown. The glitch activity of pulsars as young as the Crab ($\tau_c \sim 1$ kyr) appears to be lower than that of slightly older objects but still large compared to the rest of the sample.

5.3 Glitch sizes

5.3.1 Frequency jumps

The distribution of the fractional quantity $\Delta\nu/\nu$ of all detected glitches, shown in Fig. 2, spans almost 8 decades and exhibits two gaussian-like overlapping peaks, suggesting that glitch sizes follow a bimodal distribution. However, given the difficulties associated with finding a general lower limit for glitch detection, the completeness of the lower end of the histogram is not clear, and the current left edge of the first peak could change substantially if many small glitches were found close to the present limit of detectability.

The same bimodal behaviour is also found in the distribution of the glitch frequency jumps $\Delta\nu$, shown in the histograms in Fig. 13. In this plot, to study the details of the distribution, data were binned using two different bin sizes; either one half a decade wide, or a quarter of a decade wide. It can be seen that the overall distribution is composed of a wide component covering almost the whole range of $\Delta\nu$ values plus a very narrow peak, centred around $\Delta\nu \sim 25 \mu\text{Hz}$, involving the largest jumps.

The contribution of the 6 magnetars that have been reported to glitch is also shown in Fig. 13, with the small black bins. As already noticed by Dib et al. (2008), although their fractional sizes are all large, contributing to the height of the second peak in the fractional size histogram (Fig. 2), they spread in the $\Delta\nu$ distribution, indicating that their

clustering is only due to their very similar low rotational frequencies.

5.3.2 Frequency derivative jumps

Although measurements of $\Delta\dot{\nu}$ may not be extremely accurate, for large glitches they are likely to be fairly well estimated. Most estimates of $\Delta\dot{\nu}/\dot{\nu}$ are positive, as expected if glitch recovery is understood as an exponential-like decrease to pre-glitch values. Nonetheless, a small number of measurements are negative. Most of these are barely significant values or they may be the result of sharp features in timing noise (Lyne et al. 2010), which have masqueraded as glitches.

In Fig. 14 the frequency jump $\Delta\nu$ is plotted against the corresponding jump in frequency derivative $\Delta\dot{\nu}$. The plot includes 288 glitches, using black dots for positive $\Delta\dot{\nu}$ values. It is found that in general the two quantities correlate, indicating that large frequency jumps are generally accompanied by large frequency derivative jumps. The same glitches forming the narrow component in the $\Delta\nu$ distribution are also clustered in this plot, and also show large $\dot{\nu}$ jumps.

5.3.3 Identifying pulsars responsible for the large glitches clustered in the $\Delta\dot{\nu}$ – $\Delta\nu$ plot

To identify the objects responsible for these large glitches, all pulsars having undergone at least one glitch with a size contained in the range 10 to 45 μHz , and accompanied by a $\Delta\dot{\nu}$ jump between -450×10^{-15} and $-10 \times 10^{-15} \text{ Hz s}^{-1}$, were selected. These criteria identified 20 pulsars, which have had a total of 57 glitches satisfying the above restrictions. The selected pulsars are listed in Table 6, where the number of glitches satisfying the selection criteria are indicated for each pulsar, compared to the total number of glitches observed in that particular object. The restrictions in $\Delta\nu$ and $\Delta\dot{\nu}$ come from visual inspection of the $\Delta\nu$ distribution and the $\Delta\dot{\nu}$ – $\Delta\nu$ plot (Fig. 14). Glitches with a positive $\dot{\nu}$ jump were not considered in the selections.

The pulsars selected are highlighted in the P – \dot{P} diagram

Table 5. Glitch spin-up rate of pulsars grouped in different ranges of characteristic age.

$\langle \tau_c \rangle$ (Kyr)	$\sum T_i$ (yr)	N_g	N_{pg}	N_p	$\sum \sum \Delta \nu_{ij}$ (μHz)	$\dot{\nu}_{\text{glitch}}$ ($10^{-15} \text{Hz s}^{-1}$)
1.6	63	28	4	4	35	18(1)
6.9	65	37	7	8	530	256(7)
18.9	244	90	14	18	830	108(1)
64.9	349	53	16	29	260	23.3(4)
1.9×10^2	702	30	11	49	23	1.02(3)
5.9×10^2	1182	25	15	82	46	1.23(5)
1.9×10^3	1860	31	16	118	9.5	0.162(5)
5.6×10^3	2319	20	15	141	3.4	0.046(2)
1.8×10^4	1994	3	3	119	0.0036	0.00006(2)
6.1×10^4	1221	0	0	71	0	0
2.0×10^5	455	0	0	24	0	0
5.6×10^5	272	0	0	21	0	0
1.8×10^6	34	0	0	6	0	0
5.7×10^6	482	0	0	34	0	0
1.9×10^7	73	0	0	7	0	0

Table 6. Pulsars selected by their glitch $\Delta\nu$ and $\Delta\dot{\nu}$ jumps, and the number of events (n) satisfying the selection criteria (see text), contrasted with the total number of glitches (N_T).

PSR	n/N_T	PSR	n/N_T
B0355+54	1/6	B1800–21	3/4
J0537–6910	17/23	J1806–2125	1/1
J0729–1448	1/5	J1809–1917	1/1
B0833–45	13/16	B1823–13	3/5
B1046–58	1/3	J1846–0258	1/2
J1357–6429	1/1	B1853+01	1/1
B1610–50	1/1	B1930+22	2/3
B1706–44	1/1	J2021+3651	1/2
B1727–33	2/2	J2229+6114	1/3
B1757–24	3/5	B2334+61	1/1

in Fig. 15, which shows all pulsars with $\dot{P} > 1.65 \times 10^{-15}$. It can be seen that most selected objects are concentrated in an exclusive region of the diagram, close to the Vela pulsar, which is plotted with a black diamond. The two objects furthest apart, among the selected pulsars, are the X-ray pulsar PSR J1846–0258 (the one with the highest \dot{P}), and the relatively old PSR B0355+54 (towards the bottom of the plot). The first one has exhibited only one large glitch ($\Delta\nu = 19 \pm 1 \mu\text{Hz}$), which was accompanied by magnetar-like burst activity (Gavril et al. 2008; Kumar & Safi-Harb 2008); a glitch of this magnitude was not expected in such a young pulsar. PSR B0355+54 suffered a large glitch back in 1986 (Lyne 1987) and only small events have been detected since then (those reported by Janssen & Stappers (2006)). The pulsar with the shortest period is the X-ray pulsar PSR J0537–6910, which exhibits high glitch activity, with most of its glitches having large $\Delta\nu$ and $\Delta\dot{\nu}$ jumps. The diagram includes 2 lines of constant $\dot{\nu}$ enclosing the pulsars for which $\dot{\nu}_{\text{glitch}}/\dot{\nu} \sim 0.01$ (see Fig 11).

5.3.4 Cumulative distributions of glitch sizes

Whether an individual pulsar tends to exhibit specific glitch sizes can be studied using a cumulative distribution of glitch sizes. Fig. 16 shows the cumulative distributions of $\Delta\nu$ for the 6 pulsars with more than 10 detected glitches. In

these plots we can see the probability of occurrence of any glitch size. Vela and PSR J0537–6910 appear to have an almost mono-sized glitching behaviour, while, for example, PSR B1737–30 and PSR J0631+1036 undergo glitches of almost any size with similar probability. This is reflected in the fits performed by Melatos et al. (2008), where Vela and PSR J0537–6910 stand out, by producing comparatively small exponents for the fitted cumulative distributions. According to that work, different exponents are expected, as they would reflect, among some universal properties, the internal temperature of the star. Despite this, they acknowledge that Vela and PSR J0537–6910 exhibit exceptional glitch size distributions.

The $\Delta\nu$ distributions also show that in general Vela and PSR J0537–6910 undergo glitches with frequency jumps about 10 times larger than all glitches in the other 4 pulsars. However, we are unable to know whether we have observed these 4 pulsars long enough to securely say that they do not undergo larger glitches. Neither Vela nor PSR J0537–6910 are possible to observe at Jodrell Bank, but we believe that all jumps larger than $0.1 \mu\text{Hz}$ and $0.5 \mu\text{Hz}$ have been detected for these two objects, respectively. Vela is an extremely bright source at radio wavelengths, resulting in good signal to noise, and the smallest glitch reported has $\Delta\nu = 0.1 \mu\text{Hz}$ (Cordes et al. 1988). In the case of PSR J0537–6910, with the information available (Marshall et al. 2004; Middleditch et al. 2006) it is possible to infer that all frequency jumps larger than $0.5 \mu\text{Hz}$ have probably been detected. These limits ensure that their cumulative distributions are in fact thin and sharp.

6 DISCUSSION

In order to discuss the results in terms of a popular glitch model, a brief description of that model is presented in the next section. The following sections discuss the results.

6.1 Physics of a glitch

There are two main models describing the origin of glitches. The first regards glitches as star-quakes, produced by rear-

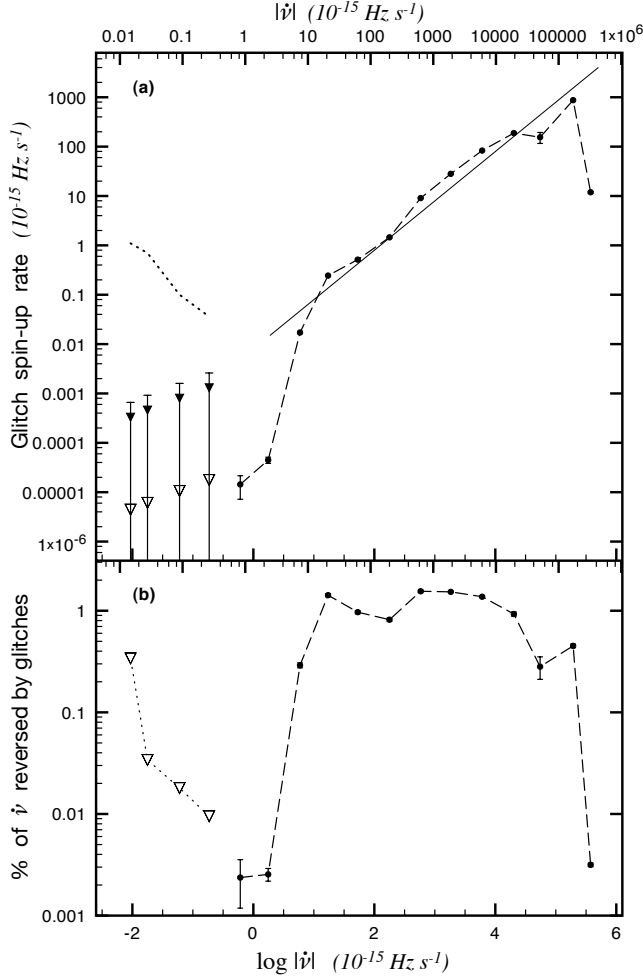


Figure 11. Glitch spin-up rate versus the slowdown rate $|\dot{\nu}|$ (top), and the percentage of $\dot{\nu}$ reversed by glitch activity versus the slowdown rate (bottom). The straight line in the upper plot has a slope equal to 1 and is not a fit to the data. For low $|\dot{\nu}|$ values, upper limits for the spin-up rate were estimated assuming that one glitch with size $0.03 \mu\text{Hz}$ (black triangles), or $0.0004 \mu\text{Hz}$ (white triangles) happened during the time necessary to have detected at least one glitch, according to a glitch rate extrapolated from the rest of the population (Fig. 10). The dotted line represents the spin-up rate if one glitch with $\Delta\nu = 1 \mu\text{Hz}$ was in the data of the pulsars in each bin. The percentage of $\dot{\nu}$ reversed by the simulated glitch activity plotted with white triangles in the upper plot is plotted in the bottom plot, using the same symbols.

rangements of an oblate crust, which would be evolving towards a most spherical shape as the star slows down (Baym et al. 1969). Glitches in the Crab pulsar could be explained by this model, but the higher glitch activity of Vela goes beyond the maximum activity that changes of oblateness could produce (Alpar et al. 1996; Wang et al. 2000). However, glitches produced by rearrangements of the crust have not been ruled out completely, and they could still be the cause of many of the glitches observed, as they could be the trigger for the other model described below.

The second model considers the inner neutron star superfluid as a reservoir of angular momentum, which is transferred to the crust during rapid events, producing what is

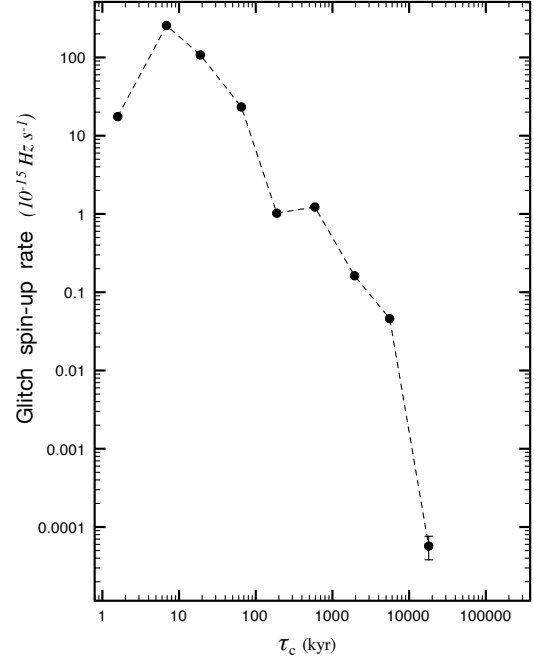


Figure 12. The mean glitch spin-up rate of pulsars versus characteristic age for pulsars grouped in semi-decade ranges of characteristic age.

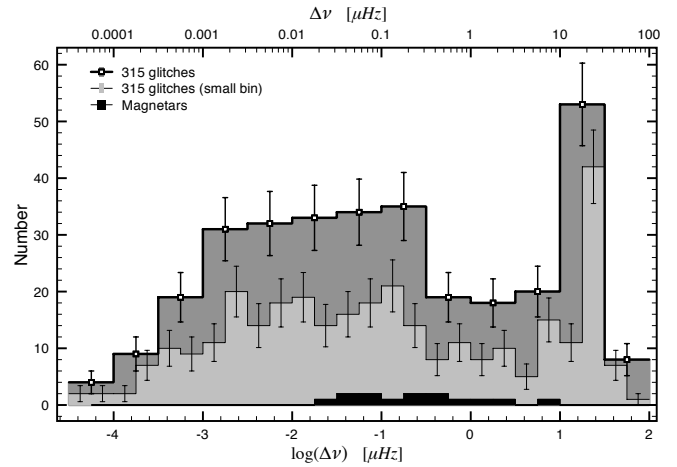


Figure 13. Histograms of the frequency jumps $\Delta\nu$ of all glitches known. Two bin sizes are used to reveal the features not visible with the larger size. Magnetar glitches are also plotted, using the small bin size and the darkest colour.

observed as a glitch (Anderson & Itoh 1975). A rotating superfluid is organised as an array of quantised vortices carrying the angular momentum of the whole superfluid body, which is proportional to the area density of vortices. Hence, if the superfluid is to be slowed down, vortices would need to move apart to decrease their density and account for the loss of angular momentum. With nothing to stop them, vortices would be expelled at the outer edge of the body, and the superfluid would slowdown normally. However, in the inner crust these vortices will find forces acting against their outward migration, impeding their normal slowdown. The

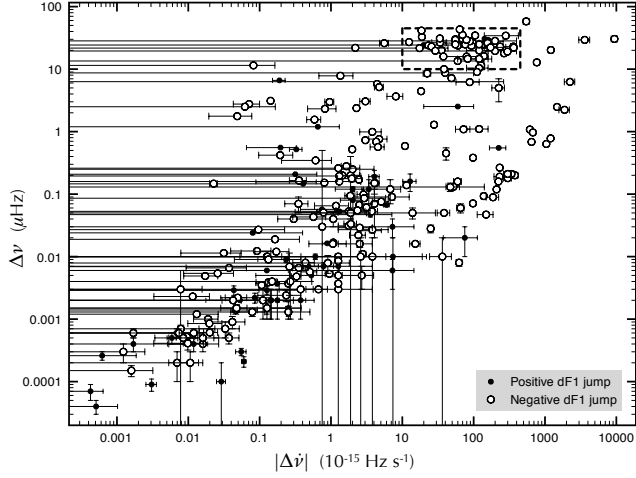


Figure 14. The frequency jump $\Delta\nu$ of 288 glitches, versus the corresponding frequency derivative jump $\Delta\dot{\nu}$. Glitches with a negative $\Delta\dot{\nu}$ are plotted in white filled circles, and those with a positive $\Delta\dot{\nu}$ are in black. The dashed rectangle encloses those events in the range $10 < \Delta\nu < 45 \mu\text{Hz}$ and satisfying $-450 < \Delta\dot{\nu} < -10$, in units of $10^{-15} \text{ Hz s}^{-1}$.

neutron superfluid of a neutron star is surrounded by a dense lattice of ions stabilised by neutrons which, due to the high densities, are also in the form of a superfluid. For the moving vortices it is beneficial, in terms of energy, to pass through the nuclei, which implies pinning there until something brakes the pinning force (Alpar et al. 1984). In particular, because the pinned superfluid is not slowing down, the Magnus force between pinned vortices and the rest of the superfluid will increase, as it is proportional to the rotation rate difference between them. For any pinned vortex, given that pinning forces are finite, the rotational lag will reach a critical value, for which the vortex will unpin and move outwards. The model developed by Alpar et al. (1984) includes two dynamically different superfluid components. One of them is continuously pinning and unpinning from the lattice, driven by thermal fluctuations (called vortex creep), or quantum tunnelling (if the temperature is too low). Therefore, this component is slowing down continuously, at the same rate as the crust slows down. The second component, involving only a small portion of the whole neutron superfluid body, is the crustal superfluid, composed of pinned vortices which will unpin only when the Magnus force is able to exceed the pinning forces. Gradients in the pinning forces can cause over-densities of pinned vortices, defining regions with high density of vortices (trap zones) and also free vortex regions. The unpinning of vortices in one dense region could cause the liberation of vortices from other regions in an avalanche like phenomena, producing a sudden angular momentum release, that is compensated by a sudden spin-up of the crust, i.e. a glitch. The collective unpinning of vortices could also be triggered, among others, by crust rearrangements (Alpar et al. 1996; Middleditch et al. 2006; Melatos et al. 2008) or by an instability related to the inertial r modes of a rotating neutron superfluid, as recently proposed by Glampedakis & Andersson (2009). In Melatos & Warszawski (2009) the observed glitch activity of some pulsars is satisfactorily reproduced when considering

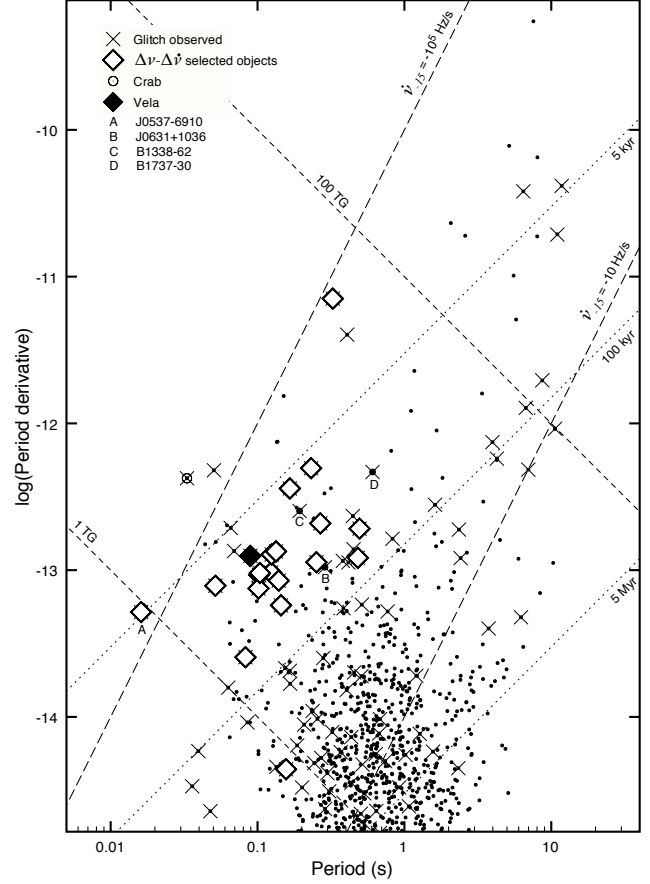


Figure 15. Top of the $P-\dot{P}$ diagram ($\dot{P} > 1.65 \times 10^{-15}$), displaying with clear large diamonds those pulsars selected in the $\Delta\nu-\Delta\dot{\nu}$ plane (Fig. 14). The Vela pulsar is highlighted using a large black diamond. In addition to lines of constant characteristic age and magnetic field, two lines of constant $\dot{\nu}$ are drawn, indicating the extremes of the $\dot{\nu}$ range for which $\dot{\nu}_{\text{glitch}}/|\dot{\nu}| \sim 0.01$.

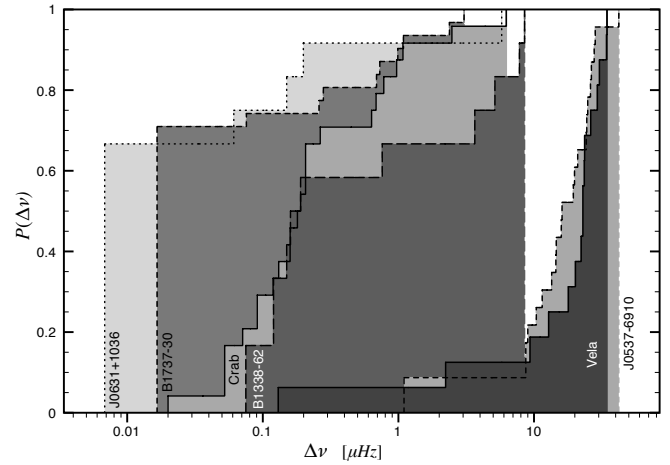


Figure 16. Cumulative distributions of glitch sizes ($\Delta\nu$) for the 6 pulsars with more than 10 detected glitches. The distributions have been normalised, and give the probability that these pulsars suffered a glitch less than a specific size.

unpinning due to thermal fluctuations and Magnus stress only, introduced as a noncritical self-organised process.

6.2 Glitch activity through the pulsar population

As previously described by other works (McKenna & Lyne 1990; Lyne et al. 2000; Wang et al. 2000), we find that the glitch activity of pulsars correlates well with $|\dot{\nu}|$ and also with τ_c . In the frame of the pinning–unpinning model, the first relationship is expected, since for a faster spindown the angular velocity lag between the crustal superfluid and the rest of the star would increase faster, being able to reach a critical value in a shorter time. Hence, provided that vortices have places to re-pin, higher spindown rates should produce higher glitch activities. However, the Crab pulsar, which has the largest $|\dot{\nu}|$ among the glitching pulsars, does not exhibit large glitches and its glitch spin-up rate is considerably smaller than that of PSR J0537–6910, which has a similar $|\dot{\nu}|$. (compare the last two rows in Table 4, corresponding almost purely to PSR J0537–6910 and the Crab pulsar, respectively).

The different glitch activity of these two pulsars could be related to age, as proposed by Alpar et al. (1996) to explain the differences between the Crab and Vela pulsars. Although the characteristic age is not an accurate age estimator, the age of the respective supernova remnants confirm that the Crab pulsar ($\tau_c \sim 1$ kyr) is younger than PSR J0537–6910 ($\tau_c \sim 5$ kyr) and the Vela pulsar ($\tau_c \sim 11$ kyr) (Comella et al. 1969; Marshall et al. 1998; Aschenbach et al. 1995). In general, very young pulsars like the Crab, with $\tau_c < 5$ kyr, undergo small or medium sized glitches ($\Delta\nu < 10 \mu\text{Hz}$), and show a glitch activity lower than older objects, like the Vela pulsar (Fig. 12). Additionally, their glitch activity seems to influence the long term spin evolution to a lesser extent; the evolution of $\dot{\nu}$ in the Crab pulsar, though interrupted by glitches, is almost linear, while in the case of Vela glitches interrupt the evolution almost completely. Perhaps higher temperatures in younger pulsars prevent the glitch mechanism from working as efficiently as it does for Vela-like pulsars (McKenna & Lyne 1990; Link et al. 1999). In terms of vortex unpinning, under higher temperatures thermal fluctuations could effectively compete against pinning forces, and impede the formation of large pinning zones. Moreover, Alpar et al. (1996) suggested that through quakes the Crab pulsar is still creating vortex depletion zones, which by the time the Crab pulsar is as old as Vela, it will behave like Vela, producing larger glitches and higher glitch activity. In this model, the current glitch activity of the Crab pulsar is driven by star-quakes. Similarly, Middleditch et al. (2006) proposed that in general young objects are just creating their first surface cracks, that generate vortex depletion and trap zones, which will later be able to produce the large glitch activity seen in objects like Vela.

The glitch activity is observed to decay steadily towards larger characteristic ages (between 5 kyr and 10 Myr), and the same decay is also observed as a function of $|\dot{\nu}|$. In the range $10 < |\dot{\nu}_{-15}| < 10^5$ (Fig. 11a), the slope of the glitch spin-up rate is very close to +1, implying a simple proportionality between glitch activity and spindown rate. In terms of vortex unpinning, this may reflect the linear dependence of the Magnus force with the velocity lag between the crust

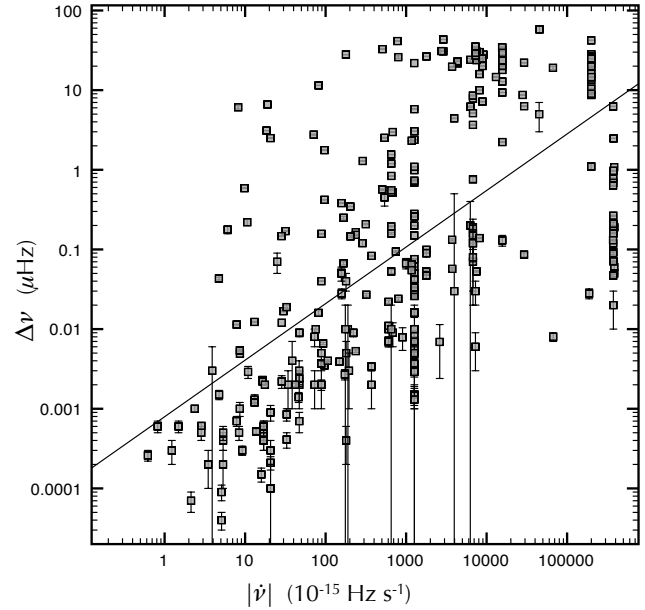


Figure 17. The magnitudes of glitch frequency jumps $\Delta\nu$ versus pulsar mean spindown rate for all glitches in Table 1. The straight line is a fit to the data and has a slope of 0.71(5).

and the neutron superfluid, supporting this model as the main mechanism producing glitches on these pulsars. In such a scenario, lower spindown rates would imply larger times between glitches, but not necessarily a decrease of glitch sizes, which depend directly on the amount of vortices that are unpinned. Consequently, no significant change in glitch size behaviour is observed for these pulsars, as inferred from the plot in Fig. 17, that shows $\Delta\nu$ versus $|\dot{\nu}|$. Moreover, a monotonous decrease on the number of glitches per year is in fact observed in the plot in Fig. 10, that shows the integrated glitching rate versus spindown rate.

While the glitching rate seems to decrease monotonically as the spindown rate does, the glitch activity presents a point where the general slope changes. This is caused by the significantly lower glitch spin-up rate of pulsars with $|\dot{\nu}_{-15}| < 10$, which appear to present an abundance of small glitches; these pulsars exhibit a large proportion of jumps below $0.001 \mu\text{Hz}$, a size that is not generally observed in higher spindown rate objects (see Fig. 17). The change in slope comes with a significant drop of the percentage of $\dot{\nu}$ reversed by glitches ($\dot{\nu}_{\text{glitch}}/|\dot{\nu}|$), from about 1% to less than 0.01%, as $|\dot{\nu}|$ decreases (Fig. 11b).

The ratio $\dot{\nu}_{\text{glitch}}/|\dot{\nu}|$ is closely related to I_{csf}/I , where I_{csf} is the moment of inertia associated with the crustal superfluid, and I is the moment of inertia involved in the normal spindown of the star, corresponding to the crust and the main superfluid bulk. Ruderman et al. (1998) assumes both ratios to be proportional, while Link et al. (1999) considers $\dot{\nu}_{\text{glitch}}/|\dot{\nu}|$ as the minimum possible value for I_{csf}/I . Hence, the amount of crustal superfluid, or its minimum amount, varies between 0.5% and 1.6% for pulsars with $-32000 \leq \dot{\nu}_{-15} \leq -10$, which corresponds to those forming the +1 slope part of the spin-up rate curve (Fig. 11). Outside this range, the portion of crustal superfluid decreases about 2 orders of magnitude.

For low spindown rate pulsars, a smaller amount of crustal superfluid would agree well with the existence of mostly small glitches; and these could be still produced by the same mechanism acting on larger spindown rate pulsars. In principle, such a situation should not produce any change on the number of glitches per year, as is in fact observed (see Fig. 10). The causes of this significant decrease of crustal superfluid may be related to a possible evolution of the trap zones, due to changes in temperature or other internal physical parameters. Two lines of constant $|\dot{\nu}|$ indicating the upper and lower limits of the +1 slope section of the glitch spin-up rate curve are drawn in the $P-\dot{P}$ diagram in Fig. 15. The line crosses the centre of the main bulk of pulsars in the diagram.

For the Crab pulsar ($\dot{\nu}_{-15} \sim 3.9 \times 10^5$) a very small amount of superfluid involved in its glitch activity may explain its relatively low glitch spin-up rate, compared slightly higher spindown rate objects (Fig. 11). In opposition to low spindown objects, glitches in the Crab pulsar are not particularly small, a fact that may support the hypothesis proposing quake-driven glitch activity on the Crab pulsar and other very young neutron stars.

6.3 Glitch size distributions

The study of the frequency jump distribution of all detected glitches showed that most glitches present a frequency jump of between 0.001 and $\sim 10 \mu\text{Hz}$ in size. Additionally, a number of events exhibit larger jumps, narrowly distributed around $\Delta\nu \sim 25 \mu\text{Hz}$. These glitches also show large $\Delta\dot{\nu}$ jumps, and are found tightly grouped in a $\Delta\dot{\nu}-\Delta\nu$ plot, almost isolated from all other glitches (Fig. 14). Most pulsars responsible for these large glitches are Vela-like pulsars, in the sense that they have similar rotational parameters, implying similar characteristic ages and magnetic fields. Those pulsars satisfying the selection criteria applied to identify these objects, but that are not Vela-like pulsars, may belong to the wide component of the overall $\Delta\nu$ distribution.

The cumulative distribution of glitch sizes in the left plot in Fig. 16 suggested that there may be two styles of glitching, leaving Vela and PSR J0537–6910 as representatives of a special class, that mainly presents glitches with a similar size, having low probability for smaller events. In contrast, pulsars like PSR B1737–30 and PSR J0631+1036 present broad glitch size distributions. Presumably, many of the pulsars selected by their $\Delta\nu$ and $\Delta\dot{\nu}$ values present sharp and narrow cumulative glitch size distributions, like Vela and PSR J0537–6910. In Table 6 the number of glitches satisfying the selection criteria per pulsar are indicated, along with the total number of detected glitches for that particular pulsar. Objects like PSR B1757–24, PSR B1800–21, PSR B1823–13 and PSR B1930+22 seem to have a large proportion of large glitches over small ones. On the other hand, PSR J0729–1448 has only had one large glitch, after 5 very small events. In general, pulsars exhibit very different glitching behaviours and it is difficult to associate them according to their glitching properties. However, Vela and PSR J0537–6910 present clear similarities that may be shared with other Vela-like pulsars, suggesting they have something in common, which is not found in the rest of the population.

While the above arguments are related to the specific values of the frequency jumps, the times between glitches

have not been considered. Vela and PSR J0537–6910 have been characterised as quasiperiodic glitchers (Link et al. 1999; Middleditch et al. 2006; Melatos et al. 2008), because their glitches occur at semi-regular intervals of time. There are indications of the same regularity between large glitches in the Vela-like pulsars PSR B1757–24, PSR B1800–21, and PSR B1823–13, with the average time between glitches varying from pulsar to pulsar. Melatos et al. (2008) analysed the size and waiting times distributions of a number of pulsars and related their glitch activity to avalanche dynamics. In this context the existence of quasiperiodic glitchers comes natural and it is seen as the result of mean-field forces dominating local interactions, which in this case would refer to the crust slowdown and thermal fluctuations.

The different glitching properties between Vela-like pulsars and other glitching pulsars with large spindown rate do not seem to be related to the amount of crustal superfluid, as these objects are well integrated in the general glitch spin-up rate trend, defined by most pulsars in the range $-32000 \leq \dot{\nu}_{-15} \leq -10$ (Fig. 11). Vela-like pulsars seem to enjoy a very stable situation, in the sense that the unpinning of a very similar amount vortices (i.e. similar glitch sizes) is produced at regular intervals of time. Other objects, like B1737-30 and J0631+1036, even though with a similar characteristic age to Vela, appear to be in a more chaotic state, where glitches of any size can happen at any time. This could be understood as an inhomogeneous distribution of pinning zones, with different pinning capacities; or as the absence (or small presence) of whichever dynamic dominates the glitch activity of Vela-like pulsars. At present, it is not clear whether these differences are part of the normal evolution in the life of pulsars, or these are exclusive properties of a different class.

7 CONCLUSIONS AND SUMMARY

A new search for glitches in the rotational behaviour of radio pulsars, using the Jodrell Bank pulsar timing database, found a total of 128 new glitches in 63 pulsars. These glitches plus those already published constitute the largest glitch database yet assembled, containing 315 glitches in 102 pulsars.

The glitch database and a sample of 622 pulsars observed for at least 3 years at JBO, were used to estimate the glitch spin-up rate ($\dot{\nu}_{\text{glitch}}$) as a function of the characteristic age (τ_c), and as a function of the first derivative of the spin frequency ($\dot{\nu}$). The glitch spin-up rate peaks for pulsars with $\tau_c \sim 5$ kyr, and as τ_c increases, the rate decreases linearly (in a logarithmic space) over 4 orders of magnitude until $\tau_c \sim 5$ Myr. For longer τ_c the glitch activity decreases with a higher rate and it disappears for $\tau_c > 20$ Myr. Towards the other end, for Crab-like pulsars ($\tau_c < 5$ kyr), the glitch activity seems to be lower than for Vela-like pulsars ($\tau_c \sim 10$ kyr), an effect attributable to higher temperatures or insufficient vortex trap capacity.

The amount of $\dot{\nu}$ reversed by the cumulative effect of glitches varies between 0.5% and 1.6% for pulsars having slowdown rates $|\dot{\nu}_{-15}|$ between 10 and 32,000, which includes all pulsars with a characteristic age between 5 and 100 kyr as well as a few other older objects (see the $P-\dot{P}$ diagram in Fig. 15, where lines of constant $\dot{\nu}$ and τ_c indicating these

limits are drawn). Towards both extremes, for faster and slower spindown rates, this ratio decreases quickly, reaching values around 0.01% (Fig. 11b). In the pinning-unpinning model these percentages may be indicative of the amount of superfluid that is involved in the glitch activity. In this context, the linear increase of $\dot{\nu}_{\text{glitch}}$ with $|\dot{\nu}|$ can be understood as a direct consequence of the linear dependence of the Magnus force with the velocity lag between the two inner components of the star.

Low spindown rates combined with small portions of crustal superfluid could explain the presence of mostly small glitches among low $|\dot{\nu}|$ pulsars. On the other hand, the glitch activity of high $|\dot{\nu}|$, or very young objects like the Crab pulsar, appears well explained by crust rearrangements, quakes or crack growing like models. In this way, despite having small portions of crustal superfluid, these pulsars could still suffer of medium sized glitches and exhibit a relatively low glitch spin-up rate, as observed.

Among the pulsars for which the percentage of the slow-down reversed by their glitch activity is around 1%, the study of glitch sizes showed that there are at least two different glitching styles. One exhibits glitches of any size, typically exhibiting $0.0001 \leq \Delta\nu \leq 10 \mu\text{Hz}$, at random intervals of time; PSR B1737–30 and PSR J0631+1036 are good representatives of this kind of activity. The other one is restricted to an almost unique glitch size, between 10 and $\sim 45 \mu\text{Hz}$, accompanied with $\Delta\dot{\nu}$ jumps in the range $-450 \times 10^{-15} < \Delta\dot{\nu} \leq -10 \times 10^{-15} \text{ Hz s}^{-1}$, and occurring at semi-regular intervals of time. The pulsars responsible for this glitch activity are mostly Vela-like pulsars, occupying an exclusive place in the $P-\dot{P}$ diagram. The differences between the glitching properties of Vela-like pulsars and some other glitching pulsars, like PSR J1737–30 and PSR J0631+1036, suggest that either there are different classes of pulsars, or there is an evolutionary trend, being a moment in the life of pulsars at which the glitch activity turns into Vela-like. In this last scenario, the evolution of the spatial distribution and relative sizes of vortex trap zones may be of relevance to explain the transition between the two different glitching styles observed.

ACKNOWLEDGEMENTS

We acknowledge the work of all telescope controllers at JBO and specially thank Chris Jordan for her help managing the observations. Pulsar research and observations at Jodrell Bank Observatory have been supported through Rolling Grants from the UK Science and Technology Facilities Council (STFC). CME thanks the support received from STFC and CONICYT through the PPARC-Gemini fellowship PPA/S/G/2006/0449.

REFERENCES

- Alpar M. A., Anderson P. W., Pines D., Shaham J., 1984, *ApJ*, 276, 325
- Alpar M. A., Chau H. F., Cheng K. S., Pines D., 1996, *ApJ*, 459, 706
- Anderson P. W., Itoh N., 1975, *Nature*, 256, 25
- Aschenbach B., Egger R., Trümper J., 1995, *Nature*, 373, 587
- Backus P. R., Taylor J. H., Damashek M., 1982, *ApJ*, 255, L63
- Baym G., Pethick C., Pines D., Ruderman M., 1969, *Nature*, 224, 872
- Camilo F., Kaspi V. M., Lyne A. G., Manchester R. N., Bell J. F., D’Amico N., McKay N. P. F., Crawford F., 2000, *ApJ*, 541, 367
- Camilo F., Manchester R. N., Lyne A. G., Gaensler B. M., Possenti A., D’Amico N., Stairs I. H., Faulkner A. J., Kramer M., Lorimer D. R., McLaughlin M. A., Hobbs G., 2004, *ApJ*, 611, L25
- Cognard I., Backer D. C., 2004, *ApJ*, 612, L125
- Comella J. M., Craft H. D., Lovelace R. V. E., Sutton J. M., Tyler G. L., 1969, *Nature*, 221, 453
- Cordes J. M., Downs G. S., Krause-Polstorff J., 1988, *ApJ*, 330, 847
- D’Alessandro F., McCulloch P. M., 1997, *MNRAS*, 292, 879
- D’Alessandro F., McCulloch P. M., King E. A., Hamilton P. A., McConnell D., 1993, *MNRAS*, 261, 883
- Dib R., Kaspi V. M., Gavriil F. P., 2008, *ApJ*, 673, 1044
- Dib R., Kaspi V. M., Gavriil F. P., 2009, *ApJ*, 702, 614
- Dib R., Kaspi V. M., Gavriil F. P., Woods P. M., 2007, *The Astronomer’s Telegram*, 1041, 1
- Dodson R., Buchner S., Reid B., Lewis D., Flanagan C., 2004, *IAU Circ*, 8370, 4
- Dodson R. G., McCulloch P. M., Lewis D. R., 2002, *ApJ*, 564, L85
- Downs G. S., 1981, *ApJ*, 249, 687
- Downs G. S., 1982, *ApJ*, 257, L67
- Flanagan C., 1991, *IAU Circ*, 5311, 3
- Flanagan C., McCulloch P. M., 1994, *IAU Circ*, 6038, 2
- Flanagan C. S., 1993, *MNRAS*, 260, 643
- Flanagan C. S., 1994, *IAU Circ*, 6064, 2
- Flanagan C. S., Buchner S. J., 2006, *Central Bureau Electronic Telegrams*, 595, 1
- Gavriil F. P., Gonzalez M. E., Gotthelf E. V., Kaspi V. M., Livingstone M. A., Woods P. M., 2008, *Science*, 319, 1802
- Glampedakis K., Andersson N., 2009, *Phys. Rev. Lett.*, 102, 141101
- Gullahorn G. E., Rankin J. M., 1978, *AJ*, 83, 1219
- Hessels J. W. T., Roberts M. S. E., Ransom S. M., Kaspi V. M., Romani R. W., Ng C.-Y., Freire P. C. C., Gaensler B. M., 2004, *ApJ*, 612, 389
- Hobbs G., Lyne A. G., Joshi B. C., Kramer M., Stairs I. H., Camilo F., Manchester R. N., D’Amico N., Possenti A., Kaspi V. M., 2002, *MNRAS*, 333, L7
- Hobbs G., Lyne A. G., Kramer M., 2010, *MNRAS*, 402, 1027
- Hobbs G., Lyne A. G., Kramer M., Martin C. E., Jordan C., 2004, *MNRAS*, 353, 1311
- Israel G. L., Campana S., Dall’Osso S., Muno M. P., Cummings J., Perna R., Stella L., 2007, *ApJ*, 664, 448
- Jackson M. S., Halpern J. P., Gotthelf E. V., Mattox J. R., 2002, *ApJ*, 578, 935
- Janssen G. H., Stappers B. W., 2006, *A&A*, 457, 611
- Johnston S., Manchester R. N., Lyne A. G., Kaspi V. M., D’Amico N., 1995, *A&A*, 293, 795
- Kaspi V. M., Gavriil F. P., Woods P. M., Jensen J. B., Roberts M. S. E., Chakraborty D., 2003, *ApJ*, 588, L93

- Kaspi V. M., Lyne A. G., Manchester R. N., Johnston S., D'Amico N., Shemar S. L., 1993, *ApJ*, 409, L57
- Krawczyk A., Lyne A. G., Gil J. A., Joshi B. C., 2003, *MNRAS*, 340, 1087
- Kuiper L., Hermesen W., 2009, *A&A*, 501, 1031
- Kumar H. S., Safi-Harb S., 2008, *ApJ*, 678, L43
- Link B., Epstein R. I., Lattimer J. M., 1999, *Phys. Rev. Lett.*, 83, 3362
- Livingstone M. A., Kaspi V. M., Gavriil F. P., 2005, *ApJ*, 633, 1095
- Livingstone M. A., Kaspi V. M., Gavriil F. P., 2010, *ApJ*, 710, 1710
- Livingstone M. A., Kaspi V. M., Gotthelf E. V., Kuiper L., 2006, *ApJ*, 647, 1286
- Livingstone M. A., Ransom S., Camilo F., Kaspi V. M., Lyne A., Kramer M., Stairs I. H., 2009, *ApJ*, 706, 1163
- Lohsen E. H. G., 1981, *A&AS*, 44, 1
- Lyne A., Hobbs G., Kramer M., Stairs I., Stappers B., 2010, *Science*, 329, 408
- Lyne A. G., 1987, *Nature*, 326, 569
- Lyne A. G., McLaughlin M., Keane E., Kramer M., Espinoza C. M., Stappers B. W., Palliyaguru N. T., Miller J., 2009, *MNRAS*
- Lyne A. G., Pritchard R. S., 1987, *MNRAS*, 229, 223
- Lyne A. G., Pritchard R. S., Graham-Smith F., Camilo F., 1996, *Nature*, 381, 497
- Lyne A. G., Pritchard R. S., Smith F. G., 1993, *MNRAS*, 265, 1003
- Lyne A. G., Shemar S. L., Graham-Smith F., 2000, *MNRAS*, 315, 534
- Lyne A. G., Smith F. G., Pritchard R. S., 1992, *Nature*, 359, 706
- McCulloch P. M., Hamilton P. A., McConnell D., King E. A., 1990, *Nature*, 346, 822
- McCulloch P. M., Klekociuk A. R., Hamilton P. A., Royle G. W. R., 1987, *Aust. J. Phys.*, 40, 725
- McKenna J., Lyne A. G., 1990, *Nature*, 343, 349
- Manchester R. N., Newton L. M., Goss W. M., Hamilton P. A., 1978, *MNRAS*, 184, 35P
- Manchester R. N., Taylor J. H., 1974, *ApJ*, 191, L63
- Marshall F. E., Gotthelf E. V., Middleditch J., Wang Q. D., Zhang W., 2004, *ApJ*, 603, 682
- Marshall F. E., Gotthelf E. V., Zhang W., Middleditch J., Wang Q. D., 1998, *ApJ*, 499, L179
- Melatos A., Peralta C., Wyithe J. S. B., 2008, *ApJ*, 672, 1103
- Melatos A., Warszawski L., 2009, *ApJ*, 700, 1524
- Middleditch J., Marshall F. E., Wang Q. D., Gotthelf E. V., Zhang W., 2006, *ApJ*, 652, 1531
- Morii M., Kawai N., Shibasaki N., 2005, *ApJ*, 622, 544
- Newton L. M., Manchester R. N., Cooke D. J., 1981, *MNRAS*, 194, 841
- Ruderman M., Zhu T., Chen K., 1998, *ApJ*, 492, 267
- Shabanova T. V., 1998, *A&A*, 337, 723
- Shabanova T. V., 2007, *Astrophys. Space Sci.*, 308, 591
- Shemar S. L., Lyne A. G., 1996, *MNRAS*, 282, 677
- Thompson C., Duncan R. C., 1995, *MNRAS*, 275, 255
- Thompson C., Duncan R. C., 1996, *ApJ*, 473, 322
- Torii K., Gotthelf E. V., Vasisht G., Dotani T., Kinugasa K., 2000, *ApJ*, 534, L71
- Urama J. O., 2002, *MNRAS*, 330, 58
- van Eysden C. A., Melatos A., 2008, *Classical and Quantum Gravity*, 25, 225020
- Wang N., Johnston S., Manchester R. N., 2004, *MNRAS*, 351, 599
- Wang N., Manchester R. N., Pace R., Bailes M., Kaspi V. M., Stappers B. W., Lyne A. G., 2000, *MNRAS*, 317, 843
- Weltevrede P., Johnston S., Manchester R. N., Bhat R., Burgay M., Champion D., Hobbs G. B., Kızıltan B., Keith M., Possenti A., Reynolds J. E., Watters K., 2010 *Publ. Astron. Soc. Australia*, 27, 64
- Wong T., Backer D. C., Lyne A., 2001, *ApJ*, 548, 447
- Woods P. M., Kaspi V. M., Thompson C., Gavriil F. P., Marshall H. L., Chakrabarty D., Flanagan K., Heyl J., Hernquist L., 2004, *ApJ*, 605, 378
- Yuan J. P., Manchester R. N., Wang N., Zhou X., Liu Z. Y., Gao Z. F., 2010, *ApJ*, 719, L111
- Yuan J. P., Wang N., Manchester R. N., Liu Z. Y., 2010, *MNRAS*, 404, 289
- Zou W. Z., Wang N., Manchester R. N., Urama J. O., Hobbs G., Liu Z. Y., Yuan J. P., 2008, *MNRAS*, 384, 1063
- Zou W. Z., Wang N., Wang H. X., Manchester R. N., Wu X. J., Zhang J., 2004, *MNRAS*, 354, 811